UNIVERSIDADE DE SÃO PAULO
ESCOLA DE ENGENHARIA DE SÃO CARLOS

JOÃO MARCELO MARIS DA SILVA FILHO

Implementation and validation of a controlled-size droplet generator

São Carlos
2024

JOÃO MARCELO MARIS DA SILVA FILHO

Implementation and validation of a controlled-size droplet generator

Bachelor's Thesis presented to the Mechatronics Engineering Program at the São Carlos School of Engineering, University of São Paulo, in partial fulfillment of the requirements for the degree of Mechatronics Engineer.

Advisor: Prof. Dr. Arthur Vieira da Silva Oliveira

FINAL VERSION

São Carlos

2024

Index card prepared by User Service at “Prof. Dr. Sergio Rodrigues Fontes Library” at EESC/USP

S586i

Silva Filho, João Marcelo Maris da
Implementation and validation of a controlled-size droplet generator / João Marcelo Maris da Silva Filho; advisor Arthur Vieira da Silva Oliveira. -- São Carlos, 2024.

Monography Bachelor Final Thesis (Undergraduate in Mechatronic Engineering) -- São Carlos School of Engineering, at University of São Paulo, 2024.

1. Droplet. 2. Hydrodynamic instabilities. 3. Image processing. 4. Real-time imaging. I. Título.

Prepared by Eduardo Graziosi Silva- CRB-8/8907

FOLHA DE AVALIAÇÃO

Candidato: JOÃO MARCELO MARIS DA SILVA FILHO

Título: Implementation and validation of a controlled-size droplet generator

Trabalho de Conclusão de Curso apresentado à Escola de Engenharia de São Carlos da Universidade de São Paulo Curso de Engenharia Mecatrônica.

BANCA EXAMINADORA

Professor Doutor Arthur Vieira da Silva Oliveira (Orientador)

Nota atribuída: 10 (dez)

(assinatura)

Professora Doutora Debora Carneiro Moreira

Nota atribuída: 10 (dez)

(assinatura)

Mestre Daniel Borba Marchetto

Nota atribuída: 10 (Dez)

(assinatura)

Média: 10 (dez)

Resultado: APROVADO

Data: 14/08/2024

Este trabalho tem condições de ser hospedado no Portal Digital da Biblioteca da EESC

SIM ☒ NÃO ☐ Visto do orientador

A Deus, por todas as bençãos providas.
Em memória de meus bisavós, Severino e Conceição.

AGRADECIMENTOS

Aos meus pais, João Marcelo e Mayra, pelo apoio e amor incondicionais; se há sucesso na minha trajetória, devo atribui-lo a vocês, que servem de inspiração e motivação diariamente. Ao meu irmão, Eduardo, pela amizade eterna; ser o seu irmão mais velho me motiva a buscar o melhor de mim, para que um dia eu possa ser a sua inspiração. Aos meus avós, tios e primos; guardo-os em meu coração.

À Júlia, por compartilhar a sua vida comigo; viver tantos momentos felizes ao seu lado me faz crer no amor, dia após dia. Aos amigos de São Carlos e do curso de Engenharia Mecatrônica, pelo apoio e parceria que transpassam os muros da universidade.

Ao meu orientador, Prof. Arthur, pela paciência e compreensão durante o desenvolvimento desta pesquisa, bem como pela amizade formada ao longo dos últimos anos; trabalhar ao seu lado foi uma experiência ímpar na minha formação científica, e pela qual sou extremamente grato.

Ao Eng. Jorge Nicolau dos Santos, pelo papel fundamental no desenvolvimento deste trabalho e de tantos outros projetos, bem como pela amizade durante os meus anos de laboratório. Ao técnico de laboratório, Florisvaldo Boni, pelo auxílio técnico na montagem da bancada e pela amizade construída. Ao Prof. Cristiano, pelo auxílio na manufatura de peças utilizadas na bancada experimental. Aos membros da banca, Profa. Debora e Me. Daniel, pela discussão de ideias e aprimoramento do trabalho. Aos meus colegas de laboratório, por toda o apoio intelectual e pessoal.

À Universidade de São Paulo, pelas excelentes estruturas de ensino e pesquisa fornecidas, as quais foram imprescindíveis na minha formação como engenheiro. À Magneti Marelli Sistemas Automotivos, divisão Powertrain (Hortolândia, SP), pela fabricação de peças utilizadas na bancada experimental. À Fundação de Amparo à Pesquisa do Estado de São Paulo pelo auxílio financeiro através dos processos #2021/01897-0, #2022/05287-5 e #2022/14365-0.

RESUMO

SILVA FILHO, J. M. M. Implementação e validação de um gerador de gotas de tamanho controlado. 2024. 80p. Monografia (Trabalho de Conclusão de Curso) – Escola de Engenharia de São Carlos, Universidade de São Paulo, São Carlos, 2024.

Gotas e sprays estão presentes em diversas aplicações industriais, desde a manufatura de telas LCD até o processo de resfriamento de placas de aço inoxidável. Muitos estudos já foram realizados sobre gotas, com uma parte significativa focada na sua geração, já que esse processo é crucial e específico para cada aplicação. Por exemplo, métodos de geração *drop-on-demand* buscam produzir uma única gota, enquanto que sistemas de trem de gotas buscam produzir uma sequência de partículas. Os princípios físicos por trás da formação de gotas também variam. Mecanismos tradicionais incluem elementos pneumáticos e piezoelétricos que pressionam o fluido contra um orifício gerando uma gota. Métodos de geração de gotas também são necessários em estudos de pesquisa fundamental. Por exemplo, o estudo do impacto de gotas requer partículas pequenas e monodispersas, o que pode ser obtido com equipamentos específicos para essas necessidades. Considerando o contexto acima, este Trabalho de Conclusão de Curso propôs a implementação e validação de um gerador de gotas com tamanho controlado. Inicialmente, foi feita uma revisão da literatura contemplando os mecanismos de geração de gota e as instabilidades hidrodinâmicas relacionadas. Então, uma bancada experimental foi construída, possibilitando testes de desprendimento de gota através da implementação de um mecanismo de aceleração forçada com um pistão pneumático. Finalmente, um modelo teórico foi proposto e comparado com os dados experimentais obtidos. O processo de validação indicou que o modelo proposto permite estimar com precisão aceitável o limiar de desprendimento da gota, corroborando o método de geração de gotas proposto. Os tamanhos de gota gerados variaram entre 522 e 2100 μm. Além disso, a geração de pequenas gotas demonstra que este equipamento poderá contribuir para o estudo do impacto de gotas realizado no grupo de pesquisa.

Palavras-chave: Gota. Instabilidades hidrodinâmicas. Processamento de imagens. Imageamento em tempo real.

ABSTRACT

SILVA FILHO, J. M. M. Implementation and validation of a controlled-size droplet generator. 2024. 80p. Bachelor's Thesis (Course Conclusion Paper) – São Carlos School of Engineering, University of São Paulo, São Carlos, 2024.

Droplets and sprays are present in several industrial applications from the manufacturing of LCD screens to the cooling process of stainless steel plates. Many studies have been conducted on droplets, with a significant portion focusing on their generation, as this process is crucial and specific to each application. For instance, drop-on-demand methods aim to generate a single droplet, whereas droplet-stream systems aim at a train of particles. The physical principles behind the droplet formation can also be varied. Traditional mechanisms include pneumatic and piezoelectric parts that pressure the fluid against an orifice generating a droplet. Droplet generation methods are also needed in fundamental research studies. For instance, the study of droplet impact requires small and monodisperse droplets, which can only be obtained with equipment specific to those requirements. Considering the context above, this final-year project proposed implementing and validating a controlled-size droplet generator. Initially, a literature review was conducted regarding the mechanisms of droplet generation and the associated hydrodynamic instabilities. Then, an experimental bench was constructed, enabling droplet detachment tests through the implementation of a forced acceleration mechanism using a pneumatic piston. Finally, a theoretical model for droplet detachment was developed and compared with the experimental data obtained. The validation process indicated that the proposed model allows an accurate estimation of the droplet detachment threshold, corroborating the droplet generation method. Detached droplets had diameters ranging from 522 to 2100 μm. Moreover, the generation of small droplets demonstrates that this equipment can contribute to the study of droplet impact in the research group.

Keywords: Droplet. Hydrodynamic instabilities. Image processing. Real-time imaging.

LIST OF FIGURES

LIST OF TABLES

LIST OF ABBREVIATIONS AND ACRONYMS

CAD	Computer-aided design
DOD	Drop-on-demand
EHD	Electrohydrodynamic
LCD	Liquid crystal display
LED	Light-emitting diode
ODF	One-drop-fill
PZT	Piezoelectric ceramic

LIST OF SYMBOLS

$\Delta\rho$	Difference of densities – [kg/m^3]
μ_l	Dynamic viscosity of the liquid – [Pa s]
ρ_g	Density of gas – [kg/m^3]
ρ_l	Density of liquid – [kg/m^3]
σ	Surface tension – [mN/m]
ϕ	Correction factor – [-]
a_f	Forced acceleration – [m/s^2]
$a_{f,min}$	Minimum forced acceleration – [m/s^2]
$a_{f,max}$	Maximum forced acceleration – [m/s^2]
Bo	Bond number – [-]
$\mathrm{Bo}_{(a_f)}$	Virtual Bond number – [-]
d	Droplet or jet diameter – [mm] or [μm]
d_0	Needle diameter – [μm]
d_{min}	Minimum droplet diameter – [mm] or [μm]
F_{ST}	Surface tension forces – [N]
g	Acceleration of gravity – $g = 9.81$ m/s^2
L	Characteristic length – [m]
m	Droplet mass – [kg]
Oh	Ohnesorge number – [-]
r	Nozzle radius – [mm]
r_d	Ratio of diameters – [-]
Re	Reynolds number – [-]
t	Time – [ms]
v	Droplet or jet velocity – [m/s]

V	Real droplet volume – [m^3]
v_f	Needle velocity – [mm/s]
W	Weight – [N]
We_g	Weber number for gas – [-]
We_l	Weber number for liquid – [-]
y	Vertical position – [mm]

SUMMARY

1 INTRODUCTION

Droplets and sprays are present in several industrial applications, especially those requiring controlled fluid volumes or high cooling rates. For example, the one-drop-fill (ODF) technology enables the manufacturing of LCD screens through the deposition of liquid crystal droplets (FAN et al., 2008). In the functioning of internal combustion engines, the injected fluid must be avoided in the chamber wall as it impairs the engine's performance and durability (MOREIRA; MOITA; PANAO, 2010). In metallurgy, sprays are responsible for cooling stainless steel plates (DOU; WEN; ZHOU, 2015). Even within the COVID-19 pandemic context experienced in recent years, studies have emerged regarding the oral droplets ejected during speech (ANFINRUD et al., 2020).

Even though they are important in industry, the study of sprays is limited because of their stochastic nature. Sprays are governed by average global parameters, neglecting local effects that may be fundamental to critical processes such as wall rewetting. On the other hand, single droplets are locally controlled and present similar governing parameters, such as droplet velocity and surface temperature – in the case of droplet impact on heated walls. Therefore, studying a single droplet may help understand the hydrodynamic and heat transfer effects in spray applications, as pointed out by Moreira, Moita e Panao (2010).

One of the main problems regarding droplet studies is their generation. Generating droplets involves working with hydrodynamic instabilities, as one must perturbate a fluid to obtain the desired fluid quantity ejected through a nozzle. The droplet generation methods are generally divided into two major groups. The drop-on-demand method is based on dripping the fluid from a nozzle and aims to generate a single droplet; the droplet-stream method is related to disturbing a jet through the amplification of the Plateau-Rayleigh instabilities and seeks to generate a train of droplets. The physical mechanism of droplet formation can vary depending on the application. Traditional droplet generators include pneumatic and piezoelectric parts that pressure the fluid against an orifice generating a droplet. Ink-jet printers, on the other hand, are almost entirely based on thermal droplet generation, in which bubble formation is utilized to eject the droplet. Minor scale methods include acoustic and electrohydrodynamic generators.

Droplet generation mechanisms are also needed in fundamental research studies. This undergraduate thesis is linked to an undergraduate research project that aimed to develop a multiple droplet generator for droplet impact experiments. The device should generate two droplets with the same diameter and impact the wall simultaneously. The droplet generation method was based on Tate's law and included accelerating the needle so a virtual body force would contribute to the droplet detachment. A theoretical model was developed and partially validated by experimental data. However, more efforts should be made to validate the model, especially by collecting more experimental points.

Considering the context above, this final-year project aimed at validating the droplet detachment model. An extensive study of the droplet generation methods and their related hydrodynamic instabilities was made. Thus, droplet generation was carried out using two main sets: a hydraulic one, consisting mainly of a syringe pump and a micro solenoid valve; and a linear pneumatic system, through which a virtual body force on the fluid mass could be done. A webcam was utilized to monitor the droplet growth in the needle, and a high-speed camera captured images of the droplet detachment. Image processing was performed using MATLAB, obtaining the droplet diameter and the needle acceleration. Finally, the results were analyzed and compared to the theoretical model.

2 LITERATURE REVIEW

2.1 Hydrodynamic instabilities

The jet breakup phenomena and its mechanisms have been studied for almost two centuries. Savart (1833) carried out experiments using an obstacle in the path of a cylindrical jet, whereas Young (1805) indicated that the surface tension plays a role in a jet breakup. Later, Plateau (1856) published his studies regarding jet formation using circular nozzles while Rayleigh (1879) and Weber (1931) wrote about inviscid and viscous liquid jets, respectively. Since then, many researchers have improved the general understanding of the area, stimulated by the technological advances conquered in the last decades, such as droplet deposition (SINGH et al., 2010), spray cooling (ZHANG et al., 2022), and spray injection systems (WU; ZHANG; ZHANG, 2021).

Traditionally, the jet breakup regimes are divided in (LIN; REITZ, 1998; LEFEBVRE; MCDONELL, 2017): i) dripping regime (low outlet velocities, which causes the accumulation of fluid in the nozzle and the generation of large droplets); ii) Rayleigh regime (higher outlet velocities, creating an axis-symmetrical jet, whose breakup is induced by surface-tension-driven instabilities); iii) first wind-induced breakup (an increase of the outlet velocity, which implicates in an early breakup thus decreasing breakup lengths); iv) second wind-induced breakup (an increase of the outlet velocity, which now leads to increasing breakup lengths) and v) atomization (even higher outlet velocities lead to the atomization regime, in which the jet breakup occurs next to the nozzle). Bonhoeffer, Kwade e Juhnke (2017) elaborated an illustrative jet breakup diagram which is presented in Fig. 1. For the dripping regime, We_l is defined as the ratio of the inertial to the surface tension forces of the liquid (DUMOUCHEL, 2008):

$$\mathrm{We}_l = \frac{\rho_l \upsilon d}{\sigma} \tag{2.1}$$

in which ρ_l, υ, d, and σ are the density of the liquid, velocity of the jet, diameter of the jet, and surface tension, respectively. For the following regimes, We_g was defined as:

$$\mathrm{We}_g = \frac{\rho_g \upsilon d}{\sigma} \tag{2.2}$$

in which ρ_g is the density of the surrounding fluid. The interfaces between the breakup regimes are represented by their corresponding Weber numbers, as the outlet velocity is increased.

In 1936, von Ohnesorge presented a study of jet breakup quantification, utilizing the Weber and the Reynolds numbers (OHNESORGE, 2019). The Reynolds number is the ratio between inertial and viscous forces and can be represented as:

$$\mathrm{Re} = \frac{\rho_l \upsilon d}{\mu_l} \tag{2.3}$$

Figure 1 – Breakup length of liquid jet for a circular nozzle as a function of the outlet velocity. Breakup regimes are identified: I) Dripping; II) Rayleigh breakup; III) first wind-induced breakup; IV) second wind-induced breakup; V) Atomization.

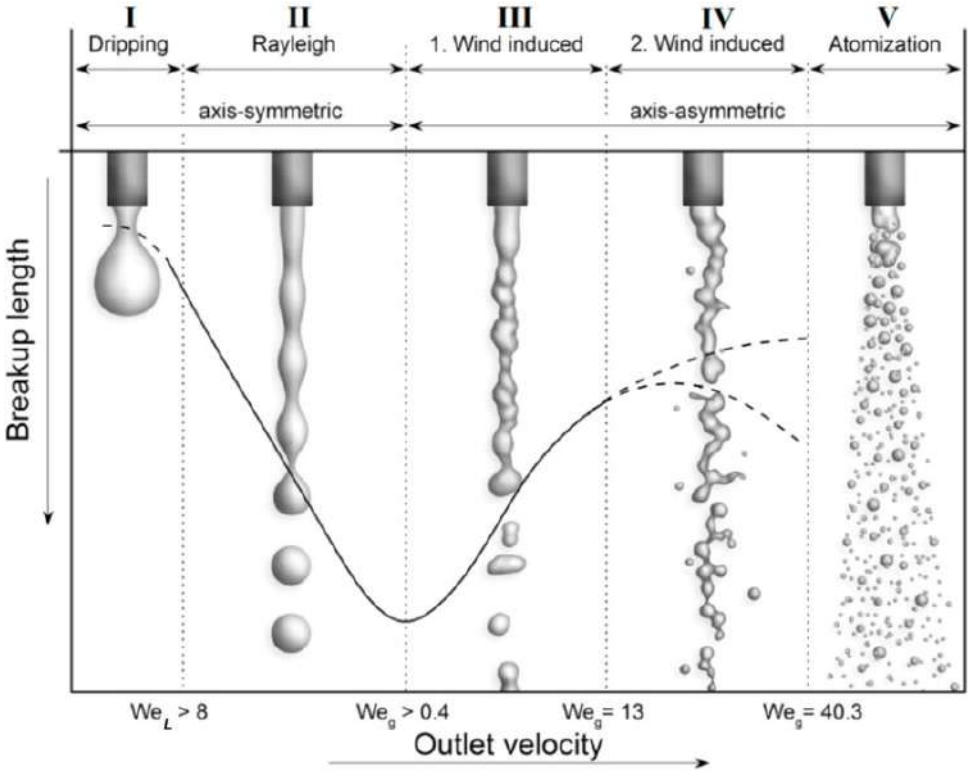

Source: Bonhoeffer, Kwade e Juhnke (2017).

in which μ_l and d are the dynamic viscosity of the liquid and the nozzle diameter, respectively. Finally, von Ohnesorge defined a new non-dimensional number that eliminated the jet velocity, being composed only of the fluid properties and the nozzle diameter. That number was entitled after his name and represents the ratio of viscous to interfacial forces:

$$\mathrm{Oh} = \frac{\sqrt{\mathrm{We}}}{\mathrm{Re}} = \frac{\mu_l}{\sqrt{\rho_l \sigma d}} \tag{2.4}$$

Figure 2 presents the Ohnesorge diagram, in which the regimes are classified utilizing the Reynolds and Ohnesorge numbers. Each liquid type has a corresponding horizontal line as the Ohnesorge number remains fixed. Baumgarten (2006) concluded that the Ohnesorge diagram is not sufficient for jet breakup prediction, since it does not consider the surrounding fluid properties. Instead, the gas density must be incorporated, as it can enhance the jet atomization (HIROYASU; ARAI, 1990). Reitz (1978) proposed the use of a three-dimensional graph, in which the gas-liquid density ratio is incorporated (Fig. 3). A more recent work (TRETTEL, 2020) discussed inaccuracies present in the Ohnesorge diagram and proposed several improvements, such as implementing the turbulence intensity as a parameter.

Figure 2 – Ohnesorge diagram for jet breakup regimes.

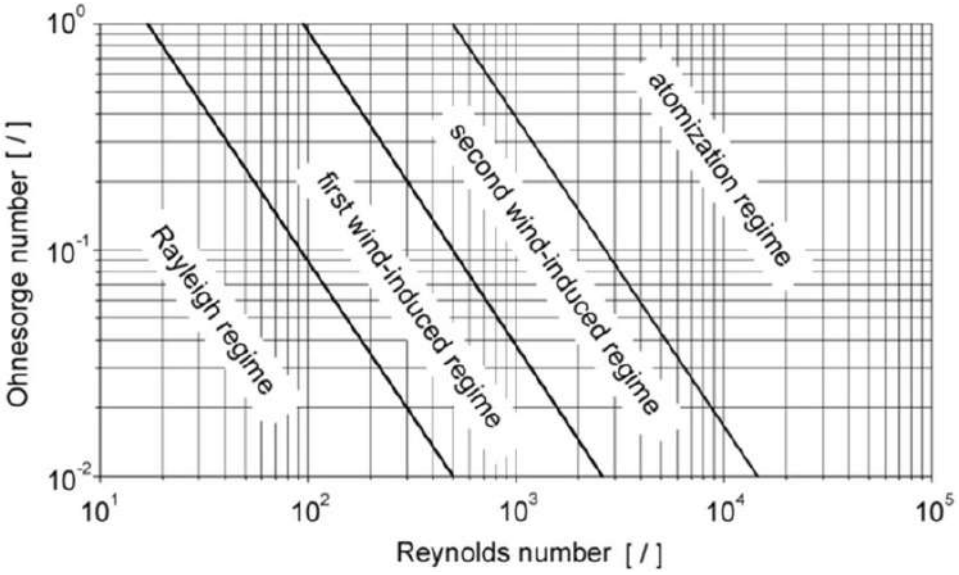

Source: Baumgarten (2006).

Figure 3 – Three-dimensional diagram for jet breakup regimes, with gas density incorporation; the Z axis represents the Ohnesorge number.

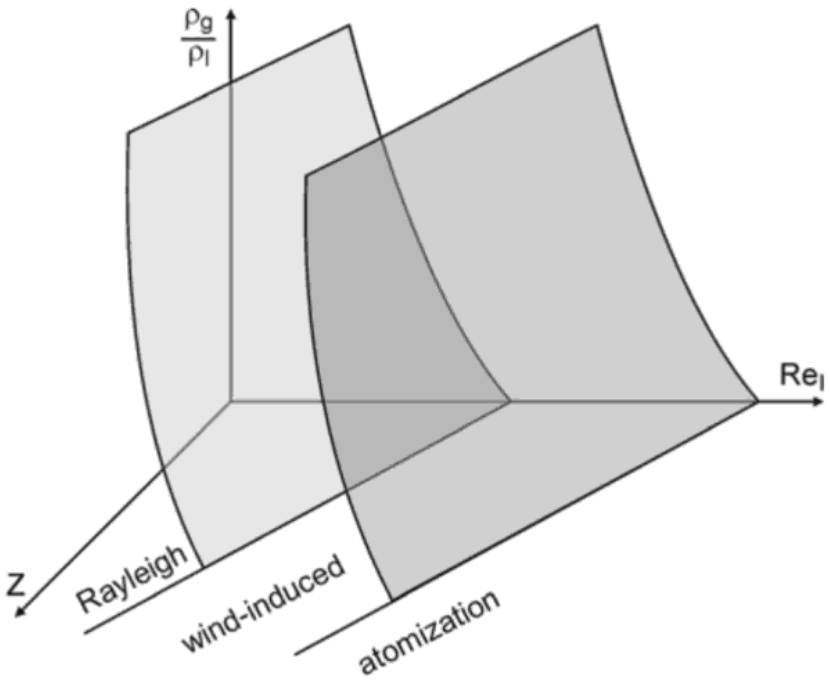

Source: Baumgarten (2006).

2.2 Droplet generation methods

The simplest way to generate a droplet involves its dripping from a capillary tube, such as a needle. As it may be noticed, droplets generated by the dripping method are considerably larger than the nozzle diameter, which is due to the high surface tension coefficients found in liquids (ASHGRIZ, 2011). Therefore, in applications that require minor droplets, the use of droplet generation devices is fundamental. These instruments must trigger hydrodynamic instabilities in a precise way so they can generate droplets with controllable sizes.

The droplet generation methods can be separated into two major groups, according to their purposes. The first one refers to the drop-on-demand (DOD) generators, which aim to produce one droplet at a time. The second one refers to the continuous-stream generators, which aim to produce a stream of droplets from a jet breakup. Both methodologies relate to the breakup regimes illustrated in Figure 1: the DOD method is based on the dripping regime, whereas the droplet-stream method is based on the Rayleigh regime. The following sections present the most common droplet generators separated by their mechanisms since some devices can generate DOD and continuous-stream droplets.

2.2.1 Piezoelectric droplet generators

Piezoelectric droplet generators have been studied for more than 50 years now in a wide range of applications (ZOLTAN, 1972; LEMKE; HIEFTJE, 1982; WANG; LIU; LAW, 1984; JIANG; UMEMURA; LAW, 1992). As the piezoelectric part is excited by a voltage pulse, the liquid suffers a positive pressure wave which ejects a portion of it through an orifice. Then, at the negative pressure moment, the fluid is drawn back so that only a detached droplet remains out of the nozzle. In the case of DOD generators, that voltage pulse is unique and produces only one droplet. In contrast, several voltage pulses are triggered in the droplet-stream methodology to generate periodic droplets.

Yang et al. (1997) successfully built a piezoelectric generator in the DOD method, using a simple system presented in Figure 4. It can be noticed that the droplet generator itself contains the piezoelectric part and the nozzle from which the droplet is detached. At the same time, the whole system is also composed of other equipment, such as a function generator and a liquid reservoir. Fan et al. (2008) presented a typical droplet generator head, which is one of the most important parts of the DOD piezoelectric system and whose body assembly is illustrated in Figure 5. They obtained good repeatability for the droplet size since for 800 droplets there was a 0.46 % volume variation.

Minov et al. (2015) proposed a piezoelectric droplet generator that can be operated in the DOD or droplet-stream methods. They overcame the problems that generally arise from the DOD method, such as aspired air bubbles, liquid pileups, and satellite droplets (KOSCH; ASHGRIZ, 2015), so they could utilize both unique and sequence voltage pulses.

Figure 4 – Piezoelectric droplet generator; the piezoelectric part is located just above the nozzle.

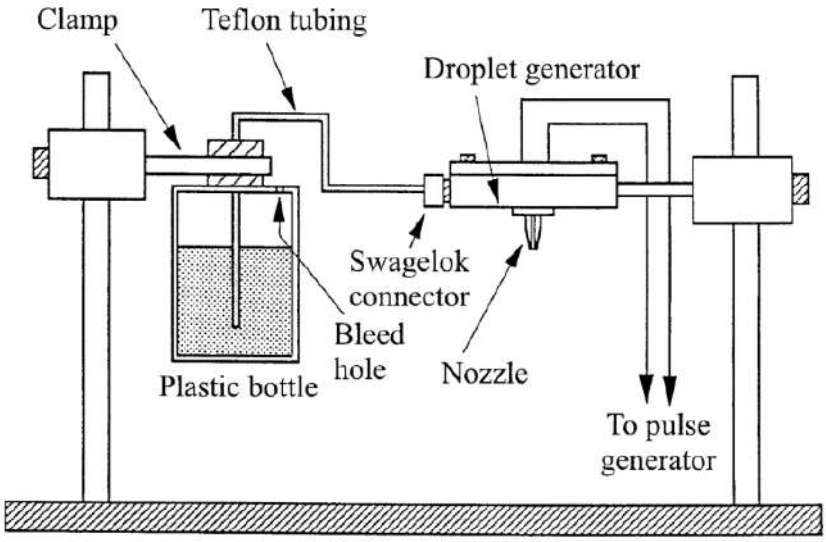

Source: Yang et al. (1997).

Figure 5 – Droplet generator assembly, utilizing a glass-made nozzle.

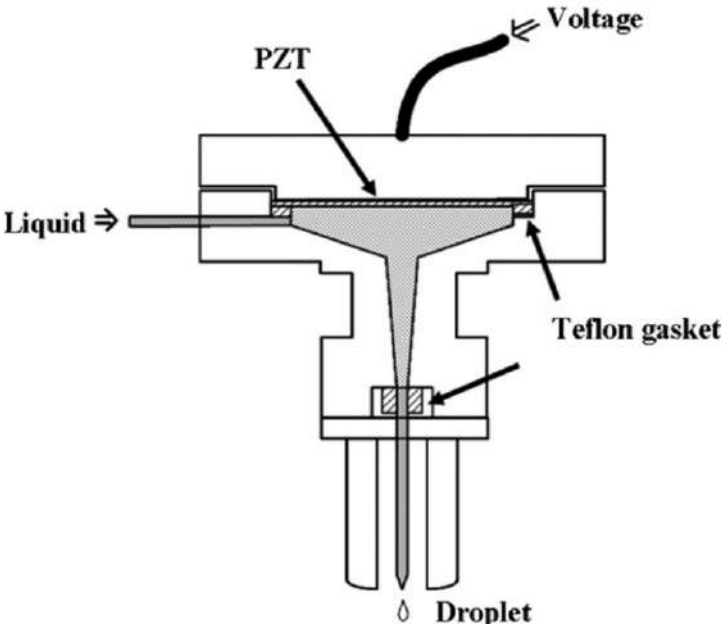

Source: Fan et al. (2008).

They tested four different nozzle diameters for each methodology and obtained droplet diameters ranging from 134.1 to 461.5 μm and 167.2 to 458.6 μm in DOD and continuous modes respectively. Figure 6 illustrates different instants of a DOD generation, in which the positive and negative voltage sequences are well exemplified in the second and third frames, respectively. Figure 7 illustrates the two different methods the authors utilized for droplet generation, with the same equipment — they only changed the voltage pulse applied to the piezoelectric part.

Figure 6 – Frame sequence of a 461.5 μm droplet formation in DOD mode. The images correspond to 0, 3, 6, 9, and 12 ms after the first frame.

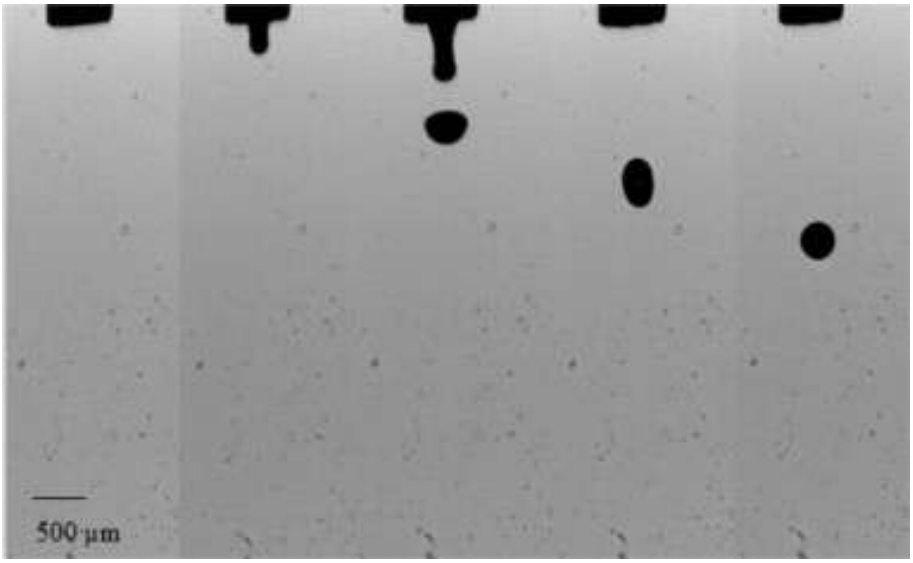

Source: Minov et al. (2015).

Figure 7 – (a) Single droplet from DOD mode and (b) monosized droplet sequence from continuous mode.

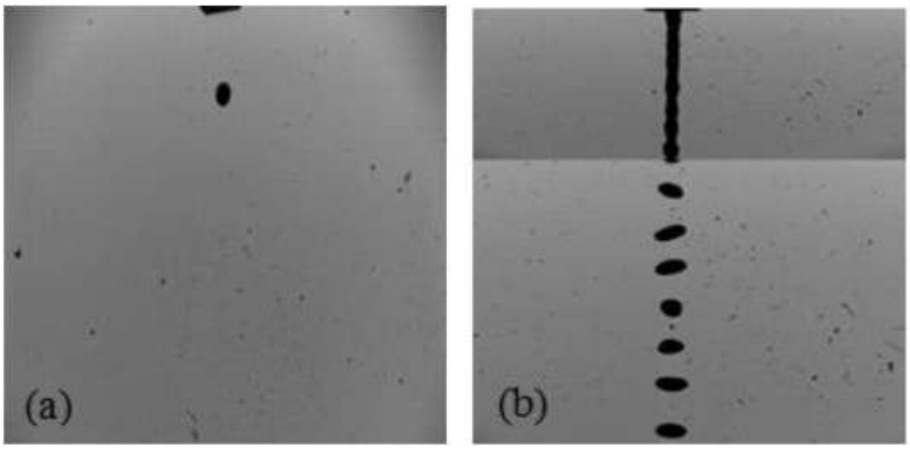

Source: Minov et al. (2015).

Some industrial applications require more than one droplet stream generation, which

can be achieved using a combined system of nozzles, as developed by Dabora (1967). However, that technique limits the distance between the droplet streams, which typically must be narrow. More recent works decreased the distance between the droplet stream by manufacturing multiple orifices in the same nozzle. Wu et al. (2020) proposed a study focused on dual stream generation using a piezoelectric device, for which they used two different size orifices in the same metal plate. Figure 8 presents the dual-stream generation system that the authors utilized.

Figure 8 – Dual-stream generation system.

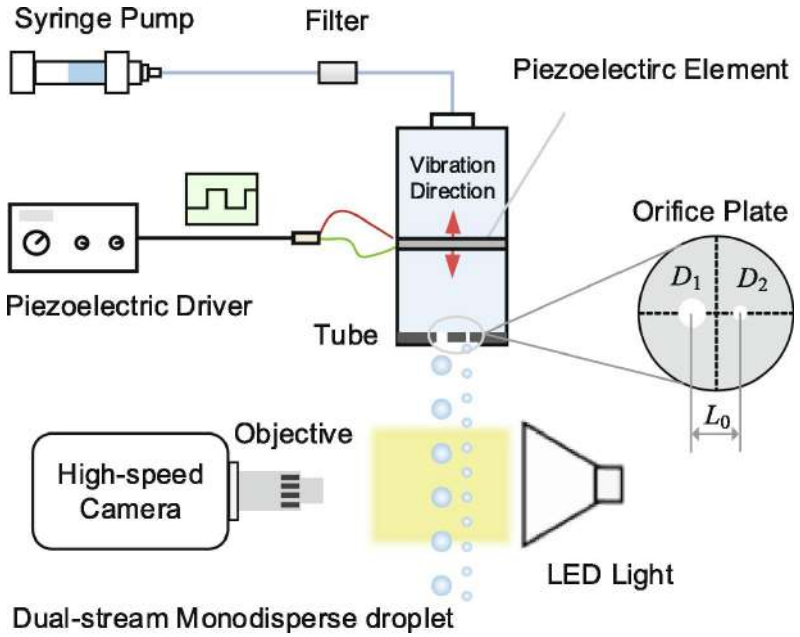

Source: Wu et al. (2020).

2.2.2 Pneumatic droplet generators

Researchers have utilized pneumatic droplet generators in several applications, from pesticide dilution in agriculture (BASI et al., 2012) to molten metal droplets in the electronic industry (CHENG; LI; CHANDRA, 2005). Those devices employ the fluid pressure of a liquid or a gas to eject a droplet from a liquid chamber. Figure 9 illustrates a well-established design for pneumatic droplet generators (CHENG; CHANDRA, 2003). As illustrated, the generator mainly includes a chamber with a bottom nozzle, which must be very small so the fluid would not exit in normal pressure conditions. Instead of using a piezoelectric part, it requires a solenoid valve which is rapidly opened and closed allowing pressure waves in the fluid inside the chamber through a T-junction. As Ashgriz (2011) mentioned, three main parameters control the pneumatic droplet generation: the solenoid pulse duration, the vent-hole size in the T-junction, and the gas supply pressure. Controlling those variables may result in a single droplet ejected per a pressure pulse.

Figure 9 – Pneumatic DOD generator chamber.

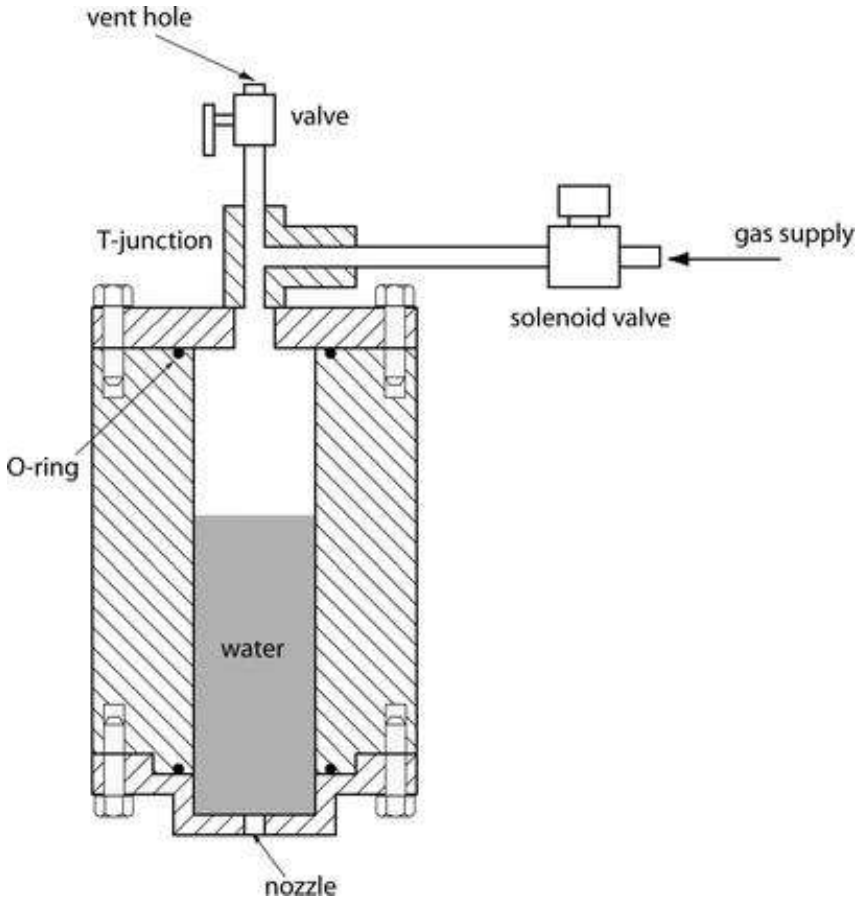

Source: Cheng e Chandra (2003).

Figure 10 presents the pressure measurements at the droplet generator cavity during a single droplet formation (CHENG; CHANDRA, 2003). The dashed line represents the solenoid pulse, which begins at $t = 0$. The pressure behavior is periodical but its amplitude varies throughout the droplet detachment time. First, after the voltage pulse wave, the chamber fluid receives a positive pressure, which ejects a thin liquid tongue through the nozzle; then, a negative pressure takes place, withdrawing the liquid; finally, as the liquid is pulled back, the jet breaks up with a single droplet detachment. The presence of negative pressure peaks in Figure 10 possibilities the generation of droplets smaller than the nozzle diameter, as Goghari e Chandra (2008) carried out in their work with glycerin mixtures. Figure 11 illustrates the pressure effects in the droplet formation. It is important to notice that very low or high viscous fluids do not enable the generation of small droplets, such as pure water (ASHGRIZ, 2011). Finally, Figure 12 presents the formation of a small glycerin mixture droplet. As the fluid jet exits the nozzle, the negative pressure peak pulls the liquid tongue back detaching a small droplet.

Figure 10 – Pressure measurements inside the droplet generator chamber for a solenoid valve pulse of 4.61 ms.

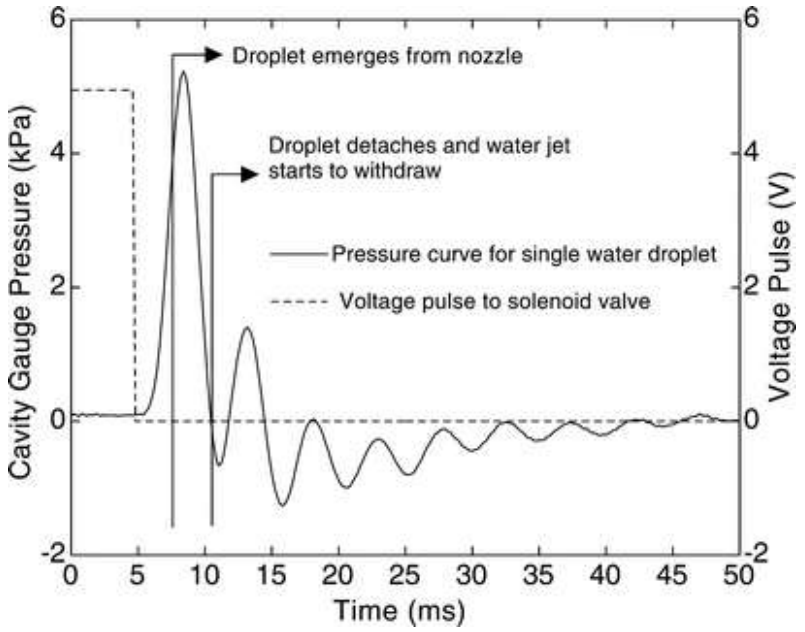

Source: Cheng e Chandra (2003).

Figure 11 – Formation steps of a droplet smaller than the nozzle size.

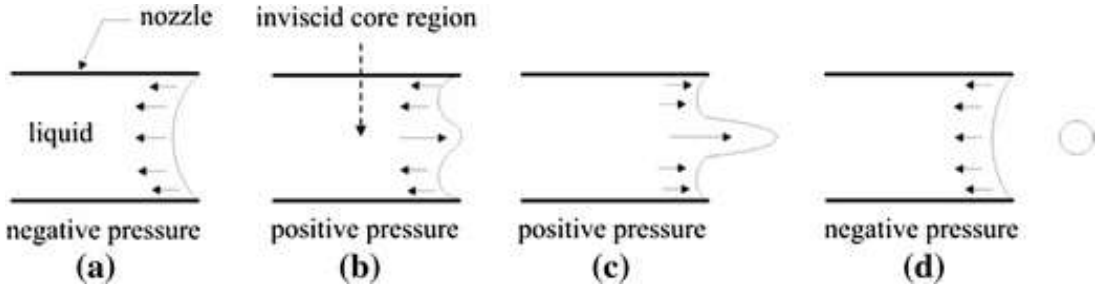

Source: Goghari e Chandra (2008).

Figure 12 – Generation of a single droplet from a 204 μm nozzle diameter, supply pressure of 69 kPa, pulse width of 5.81 ms, and exit vent tube length of 24.5 cm.

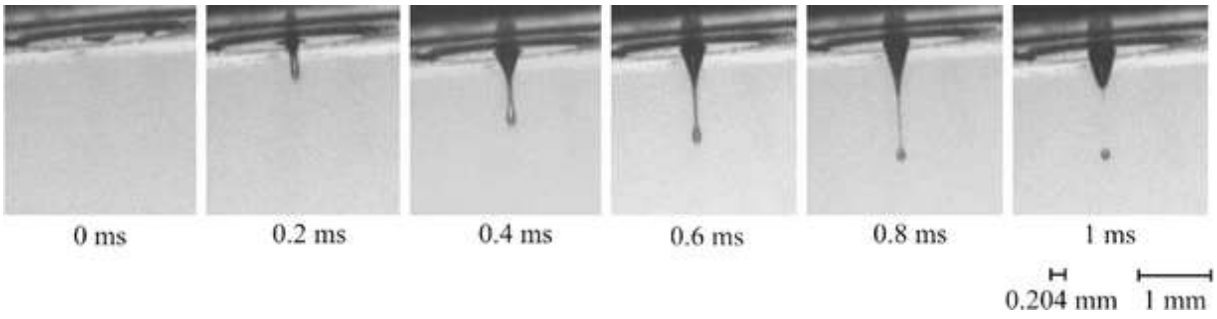

Source: Goghari e Chandra (2008).

2.2.3 Thermal or bubble jet droplet generators

Thermal droplet generators are probably the most used DOD method in the industry, considering their wide application on inkjet printers. Conversely, few related studies of their droplet generation characteristics are available in the literature especially because of the competition among the industry-leading companies (CHEN et al., 1998). Figure 13 illustrates the droplet formation process in a thermal inkjet. The common assembly includes a thermal element, a pressure chamber in which the ink remains, and an orifice. A short electric pulse activates the resistive heater, generating a high heat flux. As the ink becomes superheated, vapor formation occurs next to the heater. Then, the droplet growth triggers a pressure wave that ejects a droplet out of the orifice. Finally, after the heater is turned off, the bubble collapses creating a negative pressure that pulls the remaining liquid back into the chamber. Because of the capillary forces, the ink fulfills the nozzle again, enabling a new droplet generation.

Figure 13 – Drop formation process of a thermal inkjet.

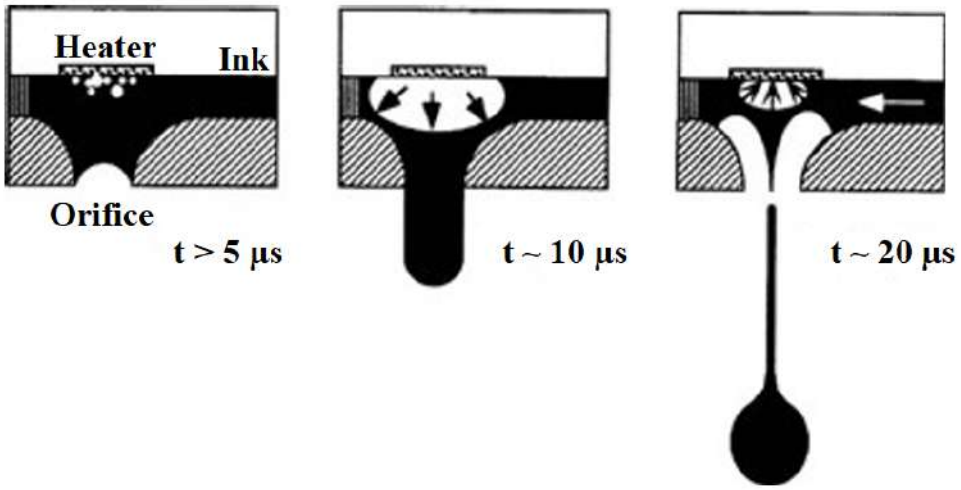

Source: Le (1998).

2.2.4 Other droplet generation methods

Beyond the main droplet generation methods presented above, other generator systems are available in the literature. The first method is the valve-based generator, utilized by Wang et al. (2022) for producing larger droplets (0.7 to 2.2 mm, for a 1 mm diameter nozzle). Figure 14 illustrates their experimental apparatus, which combines a liquid pressurization system with a solenoid valve action. Initially, the liquid is pressurized but the nozzle is closed by the action of a spring. Then, a voltage pulse activates the solenoid valve, which opens the nozzle chamber. As the fluid is pressurized, a tongue exits the nozzle during the valve opening. Finally, when the solenoid valve goes back to its original

position, the nozzle closes detaching a droplet from the ejected fluid. Figure 15 illustrates one of the results that Wang et al. (2022) obtained in their study. The droplet formation was completed after 4.2 ms while the pulse width applied to the solenoid valve lasted only 0.6 ms. Therefore, it is clear that a fast voltage pulse is necessary, to generate a single droplet.

Figure 14 – (a) Schematic diagram of the droplet generator; (b) functioning principles of the valve-base generator.

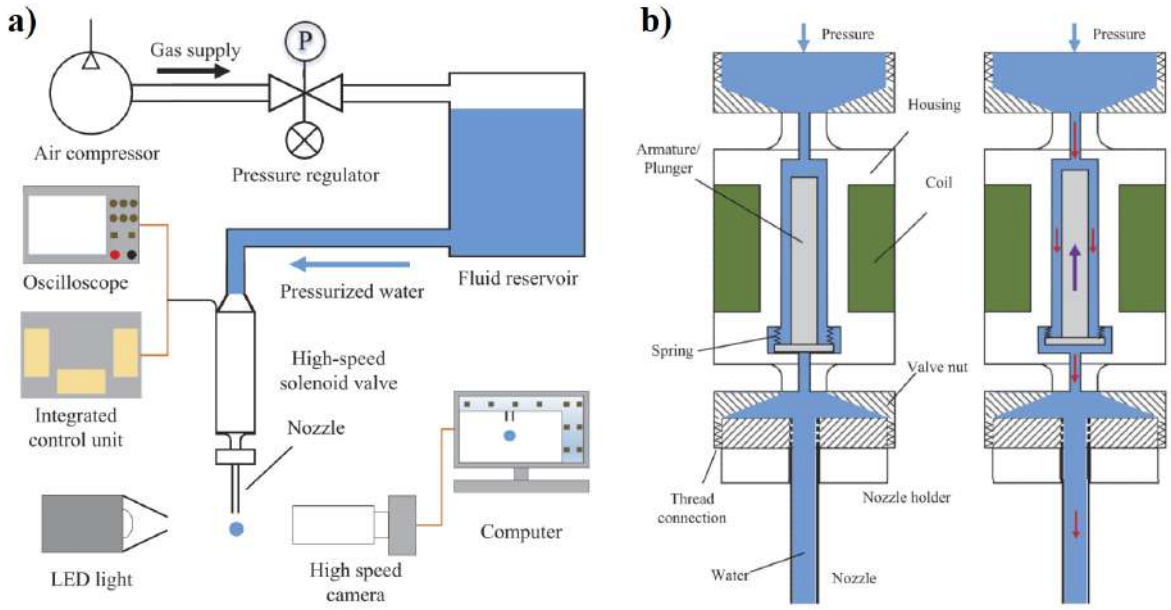

Source: Wang et al. (2022).

Figure 15 – Image evolution of droplet formation for a pulse width of 0.6 ms and applied pressure of (a) 52 and (b) 61 kPa.

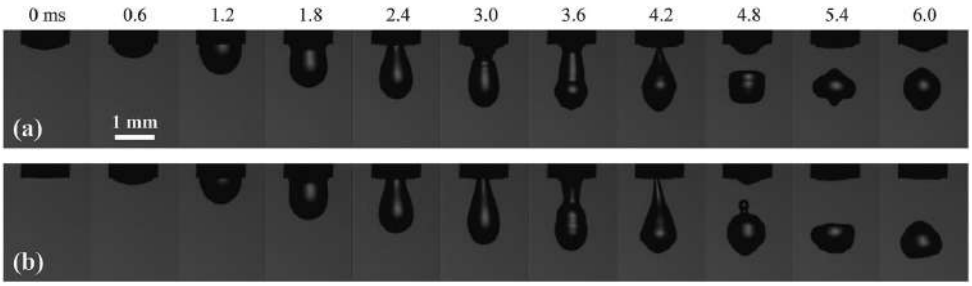

Source: Wang et al. (2022).

Donnelly e Glaberson (1966) were the first researchers to propose using a loudspeaker as a vibrating source for droplet detachment, which originated the acoustic droplet generators. Generally, those include a liquid chamber with an orifice, a thin membrane, and a loudspeaker. Through the amplification of the Plateau-Rayleigh instabilities, the authors obtained a monodispersed droplet stream as illustrated in Fig. 16.

Figure 16 – Droplet stream generation through an acoustic disturbance.

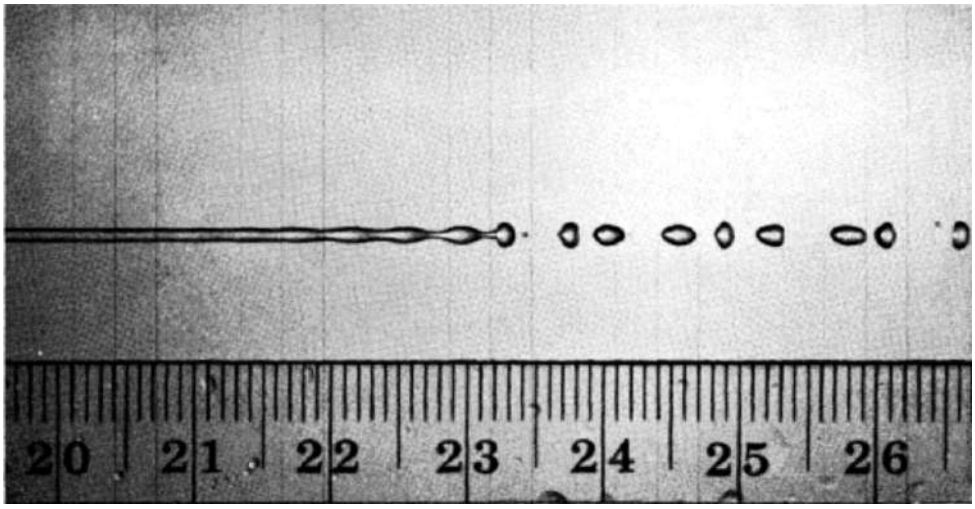

Source: Donnelly e Glaberson (1966).

Most recent studies include adaptations for the DOD method, such as the one by Castrejón-Pita et al. (2008). Figure 17 illustrates the setup utilized and the results obtained for the droplet generation. It can be noticed that the height of the fluid container must be at the same level as the meniscus in the exit nozzle. Moreover, this positioning depends on the nature of the fluid, considering its viscosity and surface tension. The droplets produced had a diameter of 1.75 mm.

Figure 17 – (a) Schematic of the DOD setup. The paraffin oil may be removed for experiments in the air;(b) photographic sequence showing the formation and ejection of a droplet of water/glycerol mixture into the air.

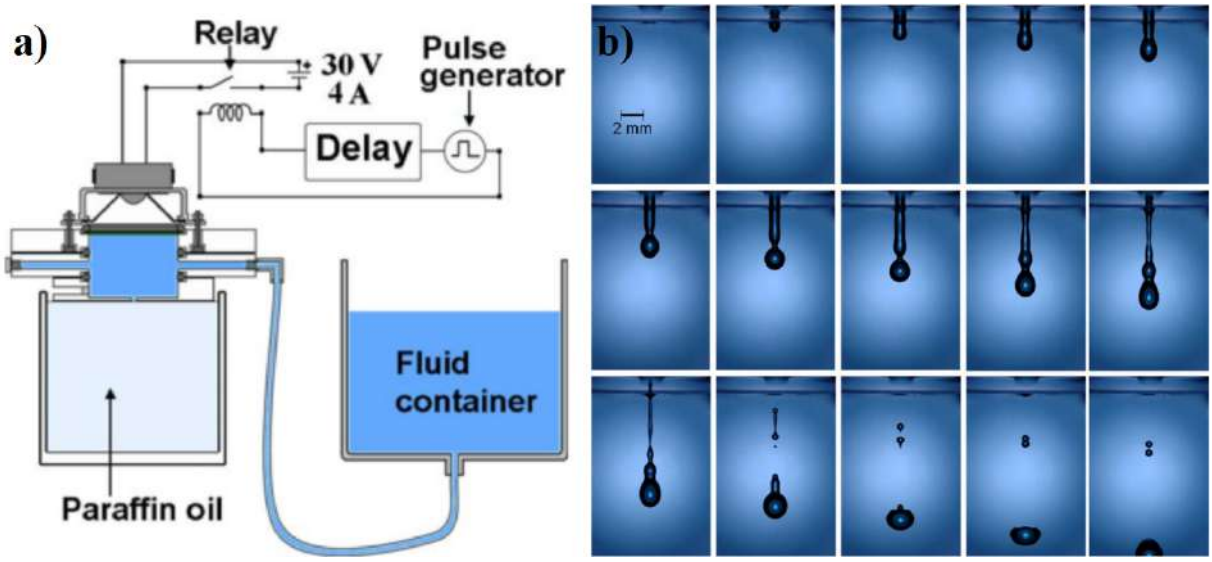

Source: Castrejón-Pita et al. (2008).

Kosch e Ashgriz (2015) pointed out that piezoelectric and acoustic droplet genera-

tion systems have limitations and disadvantages. The loudspeakers, for instance, produce sonorous noises during their vibration, which can be annoying for the operators. Moreover, robust piezoelectric systems are expensive and must be well integrated into the nozzles. In this way, the authors proposed a cheap and easy assembly vibration system, using a rotary coil actuator encountered in magnetic hard drivers. Figure 18 illustrates the assembly utilized in the studies, where the actuator vibration is responsible for the amplification of the Plateau-Rayleigh instabilities. The authors successfully produced droplets of 0.1 to 1 mm in diameter using that system.

Figure 18 – Top view of a hard drive and exploded view of the cut-out base plate, actuator arm, axis, and magnet assembly.

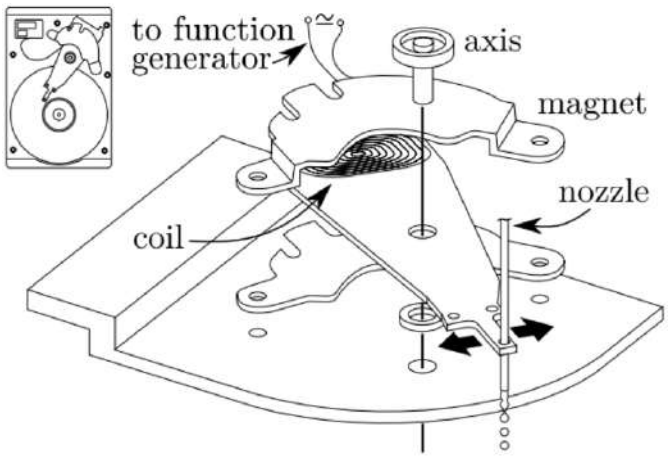

Source: Kosch e Ashgriz (2015).

The last method presented consists of the electrohydrodynamic (EHD) droplet generators. Crowley (1983), Hrdina e Crowley (1989) proposed the first theoretical study of those systems, simulating the breakup graphic profile of a liquid jet. The principle consists of an electric field acting on a nozzle surface; the meniscus is deformed in a cone shape (TAYLOR, 1968) so its bottom generates tiny droplets smaller than the nozzle. Figure 19 illustrates the flow rate and electric field strength influence in the jet breakup (COLLINS; HARRIS; BASARAN, 2007). It can be noticed that the Taylor cone formed during the electric field action can generate tiny droplets when compared to the dripping and jetting methods.

Yiwei et al. (2020) have developed a hybrid method combining the EHD and the pneumatic systems for the DOD generation. As the pneumatic assembly generated droplets, the electric field reduced their size. Previously works have utilized a pure EHD through a high voltage pulse (MISHRA et al., 2010) or a hybrid piezoelectric ejection (KIM et al., 2013). However, as pointed out by Yiwei et al. (2020), high-speed pulsed high-voltage sources are expensive, and piezoelectric actuation generates larger shear stress when compared to pneumatic systems. Figure 20 illustrates the results obtained for the hybrid pneumatic

EHD developed. The Taylor cone is present for a voltage application, which enables the generation of a smaller droplet compared to the pure pneumatic method.

Figure 19 – Flow transitions as a function of flow rate and electric field strength.

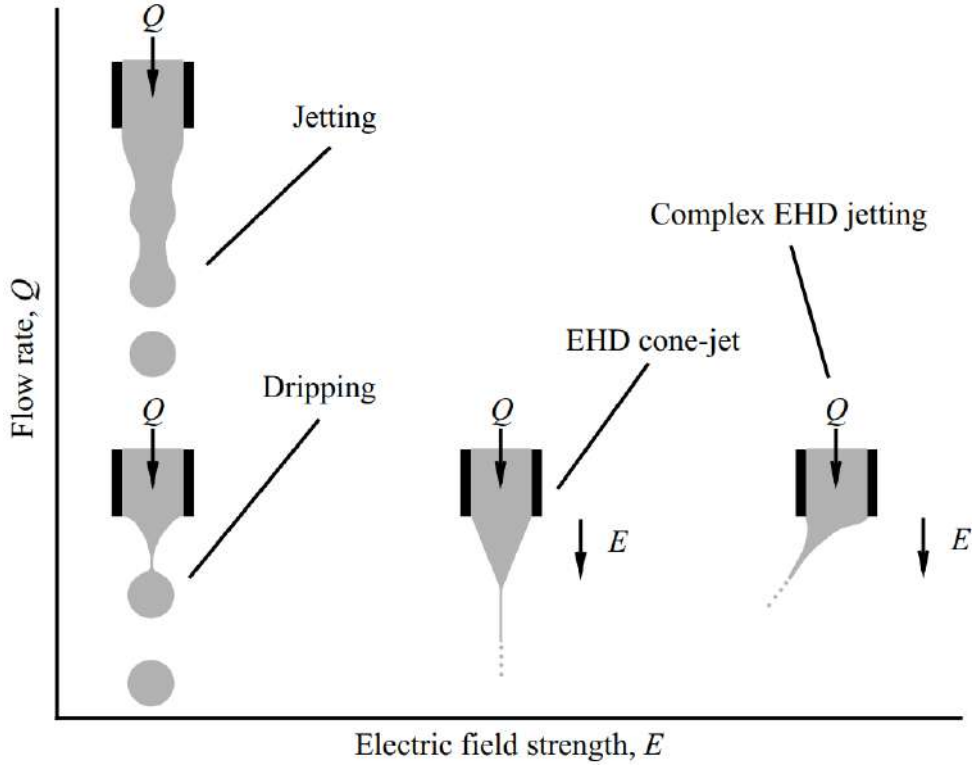

Source: Collins, Harris e Basaran (2007).

Figure 20 – (a) Ejection process for an applied voltage of 0; (b) ejection process for an applied voltage of 6.46 kV.

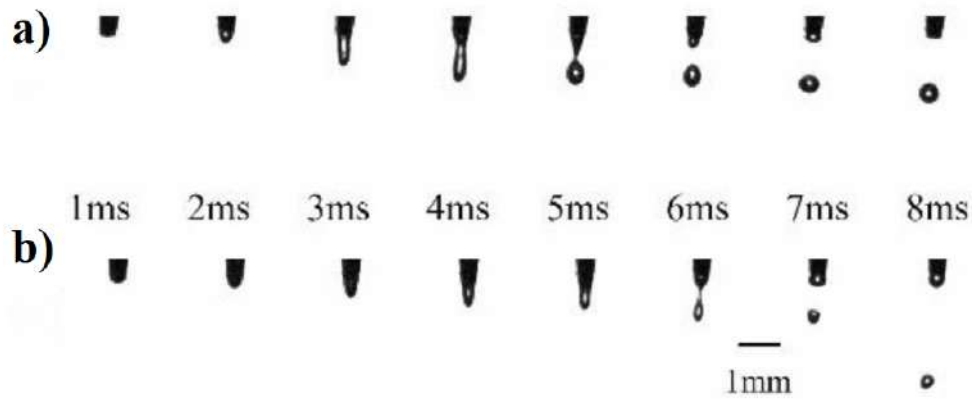

Source: Yiwei et al. (2020).

2.3 Droplet detachment (Tate's law)

The generated droplet diameter is a fundamental parameter in terms of its applications. For some presented methods, that variable must be determined empirically. In other cases, analytical equations predict the generated droplet size. Tate (1864) proposed an equation, known as 'Tate's law', for predicting the droplet diameter from the dripping method. The author utilized a balance of forces on the pending droplet, considering the weight of the liquid and the surface tension forces between the fluid and the nozzle (Figure 21):

$$mg = 2\pi r\sigma \tag{2.5}$$

in which m and r are the mass of the detached liquid and the contact radius of the nozzle, respectively. The nozzle radius depends on the nature of the fluid since its wettability will determine if the droplet is attached to the inner or outer diameter. This equation has also been utilized for surface tension determination, known as the 'drop weight method', by simply measuring the weight of a detached droplet and knowing its nozzle size (LEE; RAVINDRA; CHAN, 2008):

$$\sigma = \frac{mg}{2\pi r} \tag{2.6}$$

Figure 21 – Balance of the weight, W, and surface tension, F_{ST}, forces on the pendant droplet.

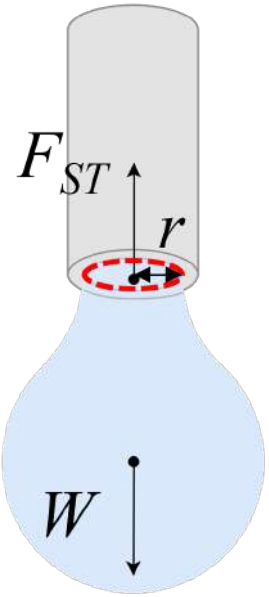

Tate's law considers an ideal scenario where all the pendant droplet mass detaches from the tip. However, the droplet breakup generally occurs below the nozzle bottom, so some mass is still adhered to the solid after the detachment. Lee, Ravindra e Chan (2009) pointed out that until 40% of the pendant mass may be left in the tip, depending on the

liquid properties and the nozzle geometry. Therefore, the Tate's law is generally utilized in the following form:

$$mg = 2\pi r\sigma\phi \tag{2.7}$$

in which ϕ is an empirical correction factor generally representing the ratio between the real and ideal droplet volumes. The parameter can also be calculated as a function of the ratio $r/V^{1/3}$, in which V is the real droplet volume. Earnshaw et al. (1996) compiled the data of several researchers (TATE, 1864; HARKINS; BROWN, 1919; WILKINSON, 1972; CARROLL et al., 1985) and used them for providing a correction factor curve. Figure 22 illustrates the curve obtained utilizing data from Harkins e Brown (1919), Wilkinson (1972). The correction factor for $0.6 \leq r/V^{1/3} \leq 1.2$ has a little variation and may provide the most accurate results as pointed out by Harkins e Brown (1919).

Figure 22 – Cubic spline approximations to the data of Harkins e Brown (1919), Wilkinson (1972). The broken line represents the manual interpolations of the combined data.

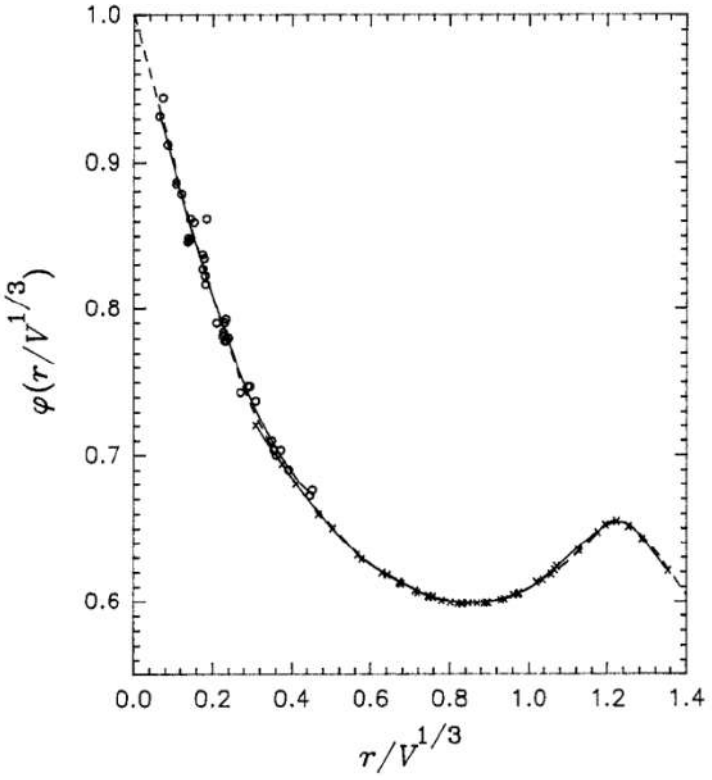

Source: Earnshaw et al. (1996).

3 METHODOLOGY

3.1 Droplet detachment modeling

In order to develop a multiple monodisperse droplet generator – i.e., an assembly that generates two identical droplets simultaneously. After discussing the available generation methods, the chosen functioning principle was the one based on the manipulation of Tate's law as follows:

$$m(g + a_f) = 2\pi r\sigma \tag{3.1}$$

in which a_f is the nozzle acceleration during the droplet detachment; the term 'forced acceleration' will be used from now on for a_f. As the needle accelerates, the pendant droplet feels a 'virtual gravity' addition, generating smaller droplets. An expression for the generated droplet size is obtained by manipulating Equation 3.1:

$$d = \left[\frac{6d_0\sigma}{\rho(g + a_f)}\right]^{\frac{1}{3}} \tag{3.2}$$

in which d and d_0 are the droplet and nozzle diameters, respectively. Therefore, increasing the needle acceleration decreases the minimum generated droplet size. Moreover, the equation does not present a correction factor, as the needle is not static – an important hypothesis for the correction factors proposed in the literature.

The next step was to find dimensionless numbers to represent the equation. Considering the forces related to the droplet detachment, the Bond number was chosen, as it represents the ratio of gravitational to surface tension forces:

$$\mathrm{Bo} = \frac{\Delta\rho g L^2}{\sigma} \tag{3.3}$$

$\Delta\rho$ and L represent the difference in density of two phases and the characteristic length, respectively. In the case of a detached droplet, the density of the air can be despised when compared to water, and the characteristic length is the droplet diameter. Moreover, the forced acceleration must be included, which provides a 'virtual' Bond number:

$$\mathrm{Bo}_{(a_f)} = \frac{\rho(g + a_f)d^2}{\sigma} \tag{3.4}$$

Manipulating the Equation 3.2, the virtual Bond number can be incorporated into the equation as it follows:

$$\frac{6d_0}{d} = \frac{\rho(g + a_f)d^2}{\sigma}$$

$$r_d = \frac{\mathrm{Bo}_{(a_f)}}{6} \tag{3.5}$$

in which r_d is the ratio of the needle diameter to the droplet diameter. As the acceleration, and the Bond number, increase, smaller droplets may be detached for the same needle size. From another perspective, the model provides the minimum magnitude of the body forces that a droplet of diameter d must have to detach from a needle of diameter d_0. Figure 23 illustrates the model plot in terms of Bo and r_d, as described in Eq. 3.5. The black line is the limit for detachment, as droplets below it detach and droplets above it do not. From the physics perspective, the body forces of the droplets above the model are not sufficient to overcome the surface tension effects. Increasing the droplet mass or the needle acceleration, the droplet is dislocated to the right in the graph until its Bond number is large enough to detachment.

Figure 23 – Graph comparison between the model and simulated experimental data for droplet detachment; colored regions indicate the model prediction – red for undetached droplets and green for detached droplets.

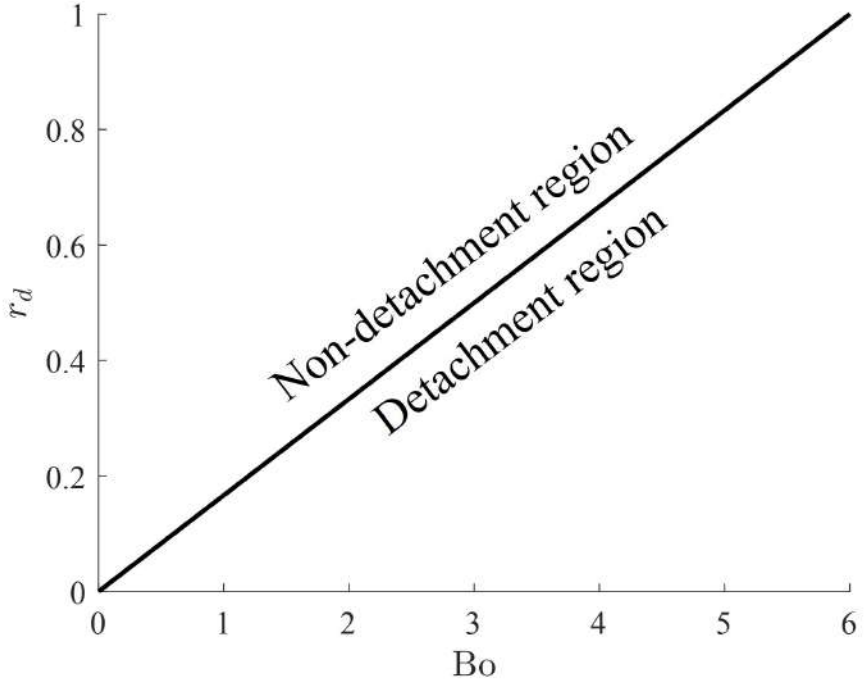

3.2 Experimental apparatus

The design of the experimental apparatus severely changed until its final version, which is illustrated in Figure 24. The mechanism of droplet generation involved accelerating the needle so a virtual force would contribute to the droplet detachment. A linear pneumatic system accelerated the needle when activated. The hydraulic set included a syringe pump, a micro solenoid valve, silicon tubes, and an industrial needle. The first two enabled the controlled fluid ejection, through real-time monitoring of the droplet growth by a

webcam. Finally, a high-speed camera (Photron NOVA S6; 6400 fps; 1024x1024 pixels) synchronized with an ns-LED light captured the droplet detachment images.

Figure 24 – Experimental setup.

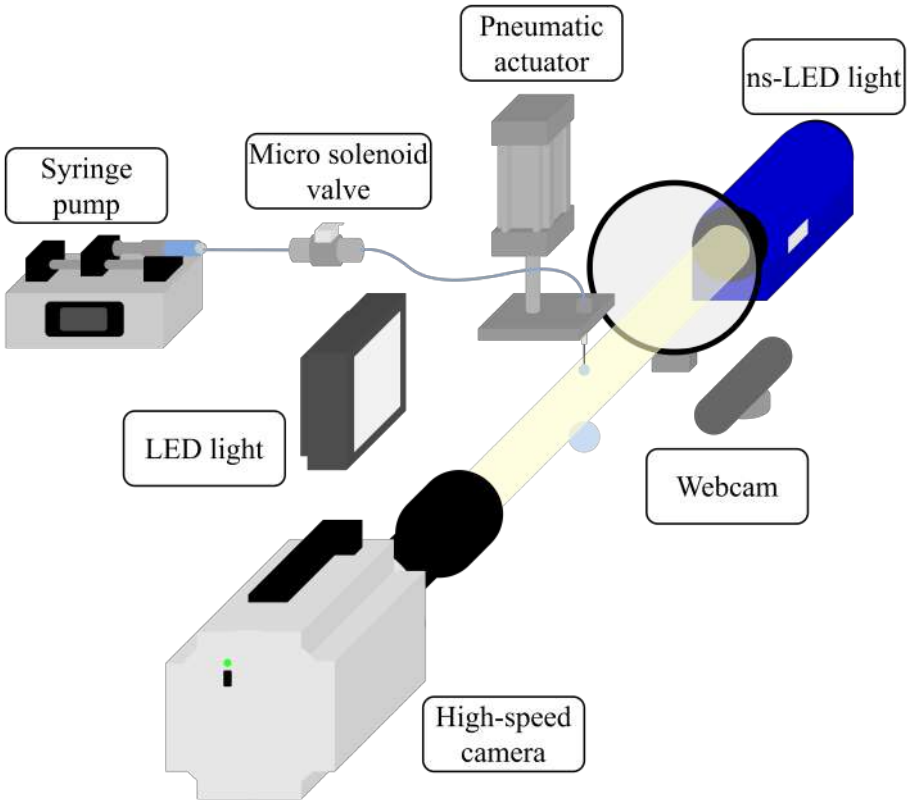

Some of the challenges encountered during the generator operation were related to the hydraulic system, which is the core of the droplet generator: trapped air bubbles disturbed the droplet generation; the first selected tubes were thick so the dislocated volume of fluid was hard to control; the first needles utilized had a diagonal cut in its tip, which influenced the solid-liquid contact area. Some solutions have been found for those problems: all the trapped air was expunged before each battery of tests; tubes with less than 90% of the previous cross-section were incorporated; industrial needles, with a flat tip, provided a reproducible droplet detachment process. Another obstacle encountered involved equipment positioning. The webcam needed to be maintained at the same distance during the experiments to conserve its configurations; moreover, the LED light should face the webcam at a specified distance to avoid excessive or short light. Aiming to solve that problem, two support parts were made by additive manufacturing, which enabled the proper assembly of the components. Figure 25 illustrates the two manufactured parts. The first was a needle plate support connected to the pneumatic piston. The second was a support piece for the webcam and LED light, remaining fixed to the cylinder base. The latter also has two holes available for a serpentine fixation, in case of future temperature-controlled experiments. Finally, Figure 26 presents the mounted assembly of the parts.

Figure 25 – CAD models: additive manufactured parts. (a) Needle plate support; (b) webcam and LED support.

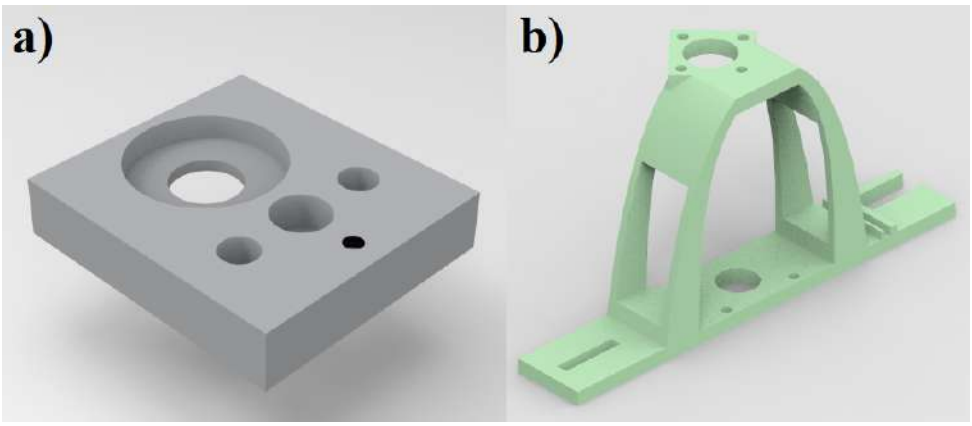

Figure 26 – Assembly of the parts for droplet size controlling.

For generating droplets of different diameters, real-time software for monitoring the droplet growth was developed. It has the purpose of providing the desired droplet size in the needle before detaching it from the needle. The code interface implemented in the LabVIEW (2013) program is illustrated in Figure 27. First, it captures the webcam images in real time; the user identifies the area of interest and the software finds the needle tip in that area; as the fluid is injected by controlling the syringe pump and the micro solenoid valve in the software, the droplet pixels are identified in the software and counted; finally, when the pendant droplet has achieved a determined area of counted pixels, the user can activate the pneumatic system by using a button in the interface. For precise predictions, a relation must be defined between the shadowed area of the droplet and its generated diameter. A method using ellipse fitting instead of pixel counting was considered but minor differences in background light undermined that method, causing its discard.

Figure 27 – Software interface utilizing for droplet size control.

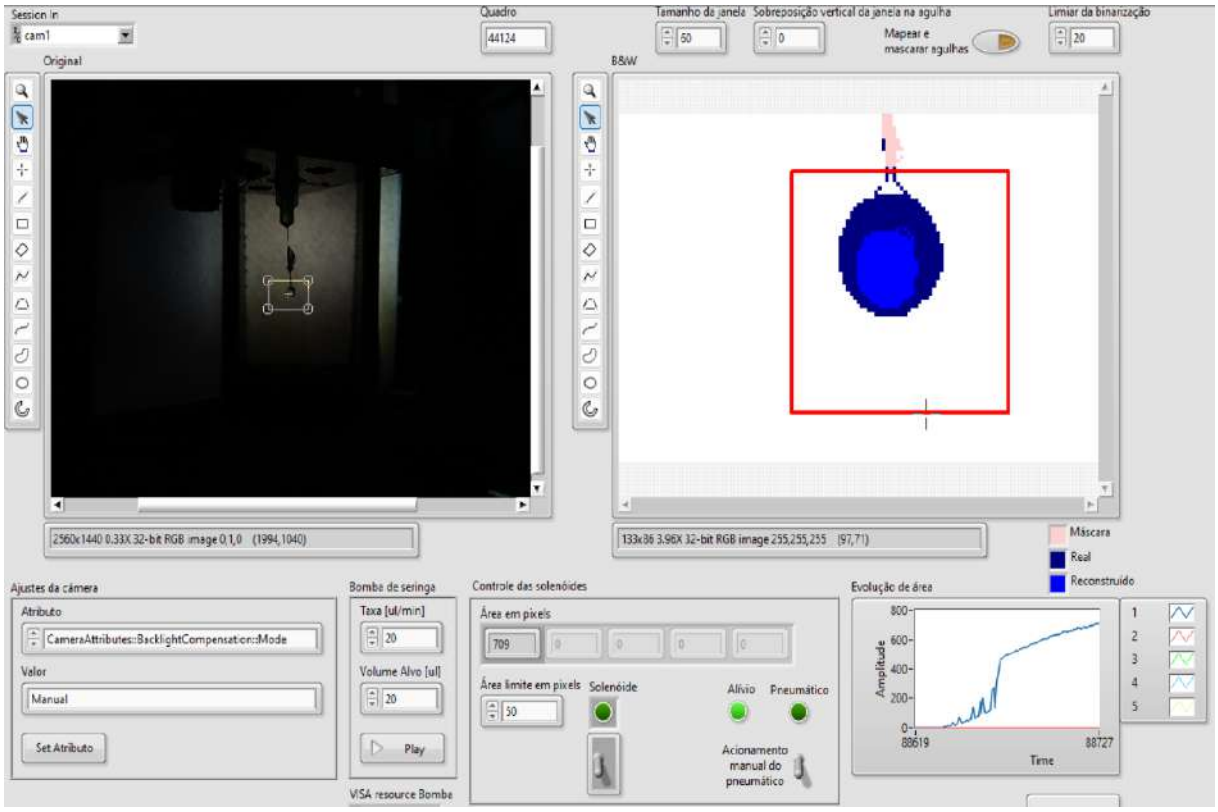

3.3 Image processing

As indicated in Section 3.2, a high-speed camera was utilized to capture images of the droplet detachment tests. The image processing consisted of codes developed in the MATLAB (R 2022b) program using native functions and own-developed routines (code

available in Appendix A). First of all, an image calibration was necessary to find the pixel size of the images. It was obtained utilizing a known-size object, such as a screw. Figure 28 illustrates one of the calibration images, where a screw head was positioned in the focus of the camera. Knowing its real size (9.84 mm) and counting the pixels in the image for the same dimension, the pixel size could be obtained for each experimental campaign, which ranged from 9.83 to 12.38 μm. The average pixel size accuracy was ± 0.2 μm.

Figure 28 – Reference object utilized for the pixel size calibration.

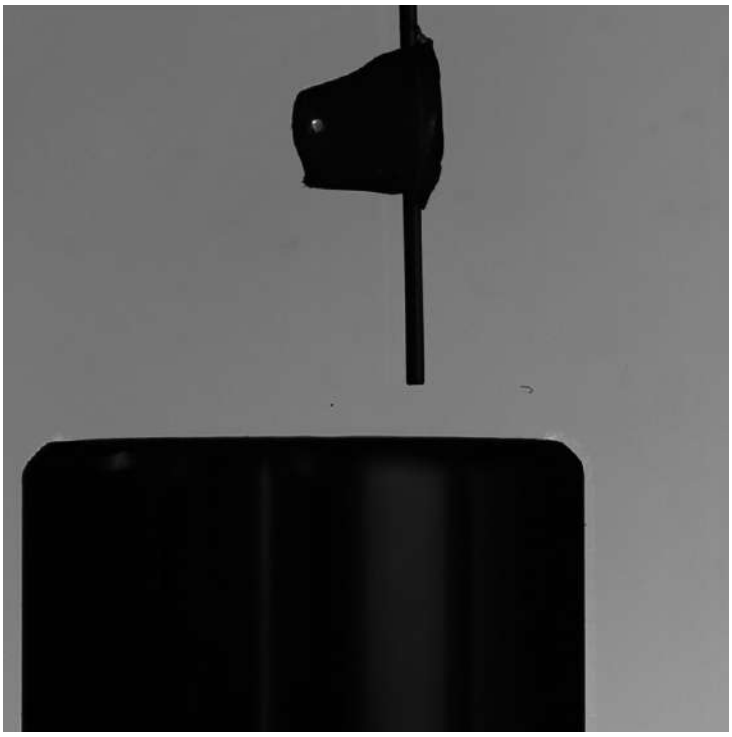

The first parameter obtained in the tests was the droplet diameter, for which the native function 'imfindcircles' was utilized. Figure 29 presents the 'imfindcircles' adjustment for detached and undetached droplets. For the undetached droplets, the measurement was made with the droplet attached to the needle, which is considered a good approximation since they are small and do not present intense deformation.

The second parameter of interest was the needle acceleration, for which an own-developed routine was utilized. Figure 30 illustrates the method, which is executed as follows: i) the images are binarized so the needle is black and the background is white; ii) the first black point in the middle line of the image (red dot in Figure 30) is detected; iii) the code reads the upward lines until it finds a black point with a horizontal distance of 40 pixels (yellow dot in Figure 30) considering the first reference point; iv) as the next frames are processed and the needle upraises, the red dot is updated utilizing the yellow dot's position of the previous frame; v) all the yellow dots' positions are stored as they represent the vertical position of the needle; vi) a fourth-degree polynomial is adjusted to the data utilizing the 'polyfit' function available in MATLAB and vii) the second deriva-

Figure 29 – Image processing utilizing the 'imfindcircles' function for droplet size characterization.

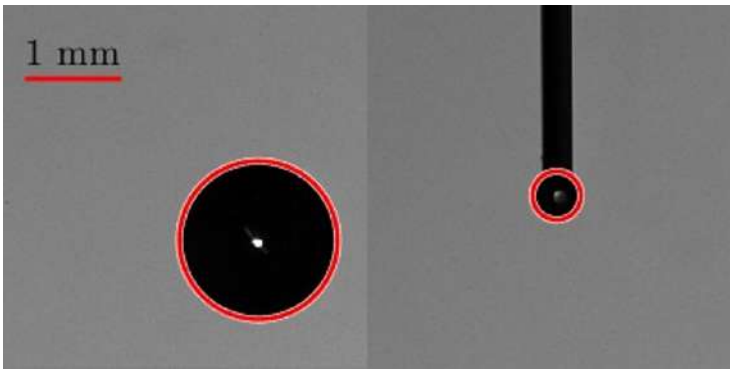

tive of the polynomial is obtained, representing the needle's acceleration through time. A fourth-degree polynomial was needed since the needle acceleration was not constant – otherwise, a second-degree polynomial would suffice.

Figure 30 – Image processing for needle acceleration capture; red arrows indicate the reference point utilized for the vertical position tracking.

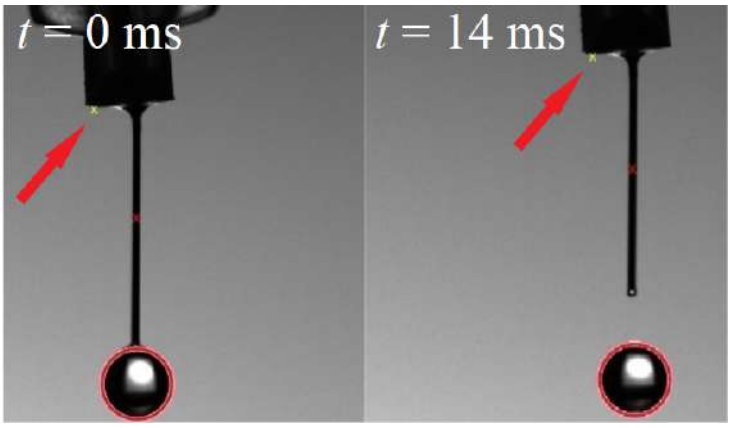

3.4 Experimental procedure

Aiming for good performance of the droplet generator, a sequence of steps was followed during the execution of the experiments: i) the tubes were filled with the desired liquid until there were no air bubbles inside; ii) the pneumatic pressure was adjusted to the desired working value; iii) the calibration frames were obtained utilizing a known-size object; iv) the fluid was injected activating the syringe pump through the LabVIEW program – at the same time, the micro solenoid valve was opened; v) as the droplet grew, the software monitored the number of droplet pixels until it reached the defined value, and the syringe pump and the micro solenoid valve were turned off; vi) then, the high-speed camera started recording and the pneumatic piston was activated; vii) the recording was saved and a preview analysis was made, in which the droplet size was estimated and viii)

finally, the procedure was repeated for another experimental point until all conditions were tested.

3.5 Uncertainty analysis

The variables presented in the physical model have associated measurement uncertainties, which must be considered in the experimental data. The uncertainties in r_d are mainly due to the needle size estimation. Table 1 presents the measurements for the outer and inner diameters of the needles utilized in the main experiments, as indicated by the supplier. It can be noticed that, for the 34G model, the inner diameter has a relative uncertainty of 83.3%.

Table 1 – Needle measurements for the outer and inner diameters.

Needle model	Outer diameter ± 20 [μm]	Inner diameter ± 50 [μm]
24G	550	300
26G	450	240
30G	300	150
34G	240	60

The uncertainties in $\mathrm{Bo}_{(a_f)}$ are mainly due to the needle acceleration measurements. The polynomial adjustment for the vertical position of the needle revealed that its acceleration was not constant during the droplet detachment. Since the needle acceleration is given as a constant in the physical model, the average value of the acceleration range was utilized. Moreover, error bars were added to indicate the maximum and minimum accelerations during the movement. Considering all experiments, the average values calculated may represent up to 18 times the minimum acceleration value. Therefore, only the needle size uncertainties and the needle acceleration ranges will be considered in this work, as they are considerably greater than any other associated errors.

4 RESULTS AND DISCUSSION

4.1 Previous data obtained for droplet detachment

During the undergraduate research project to which this work is related, preliminary experimental data were obtained to validate the droplet detachment model. Those experiments contemplated a 34G (gauge) hypodermic needle and water as the droplet fluid. Figure 31 presents images from two experiments: the minor droplet, on the left-hand side, has not detached whereas the major droplet, on the right-hand side, has detached.

Figure 31 – Frames for two experimental data, using a 34G hypodermic needle and water.

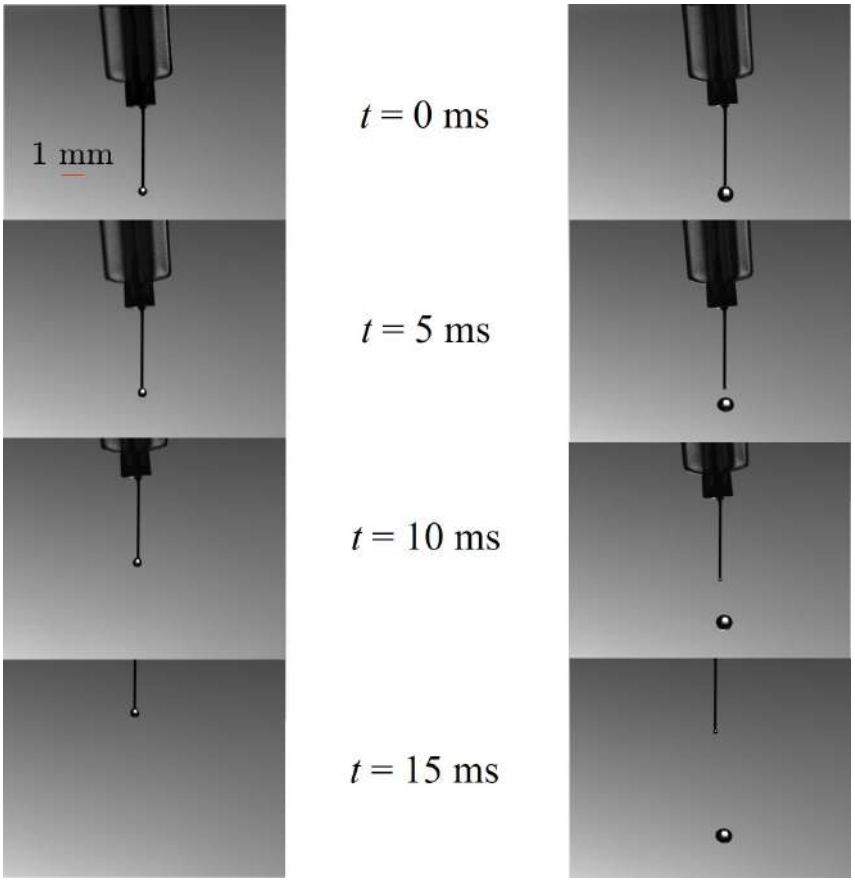

Figure 32 illustrates the needle's tracking position and the fourth-degree polynomial adjustment for one of the experiments. It is important to notice that the polynomial was adjusted considering only the interval of the needle movement, excluding the instants before the pneumatic activation. Figure 33 illustrates the needle's tracking velocity, which was calculated as the first derivative of the adjusted polynomial.

Figure 34 illustrates the needle acceleration profile for the same experiment. The curve was obtained considering the second derivative of the adjusted polynomial. For the experiments where the droplet was detached, the acceleration was calculated until the detachment frame whereas for undetached droplets the acceleration was computed for all the vertical trajectory. It is important to notice that the acceleration is not constant; therefore,

Figure 32 – Needle position during the droplet detachment for an experimental point; the red curve indicates the fourth-degree polynomial adjustment whereas the black line indicates the instant of pneumatic activation.

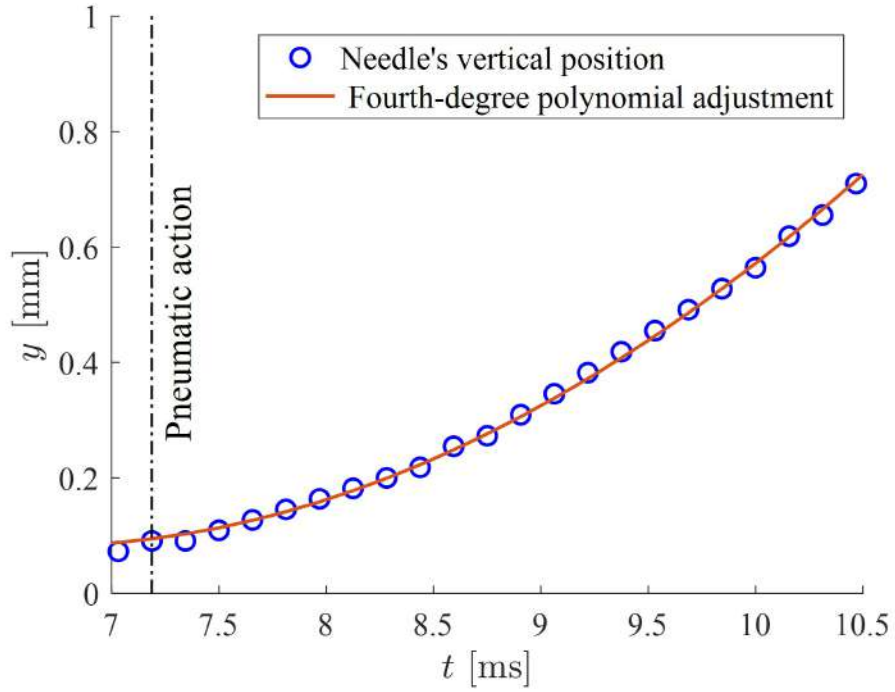

Figure 33 – Needle velocity during the droplet detachment for an experimental point; the black line indicates the instant of pneumatic activation.

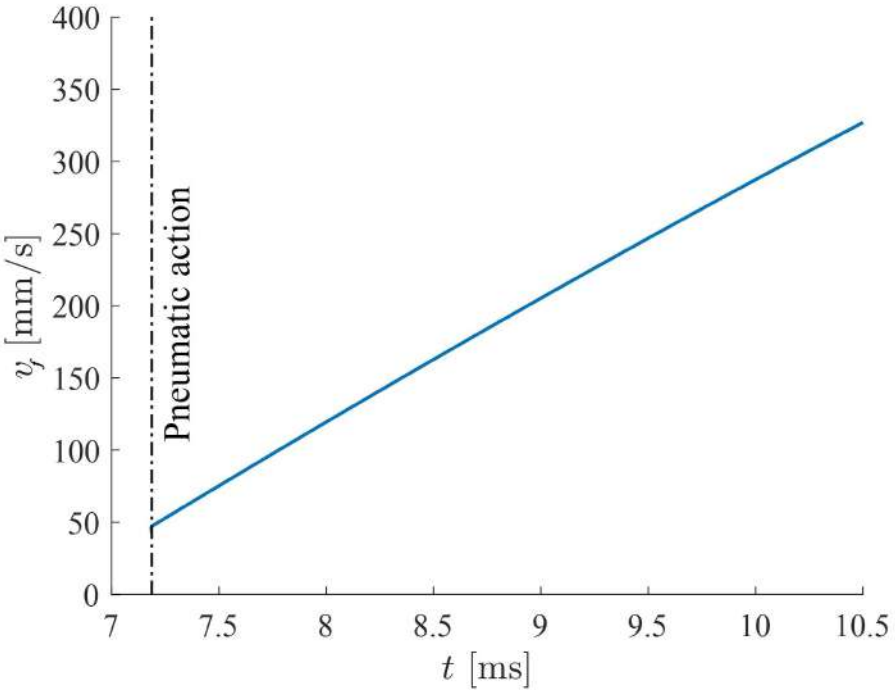

the fourth-degree polynomial is justified, as a second-degree one would not capture that information. Furthermore, the acceleration decreases over time for all the tests. Therefore, if the droplet size is close to the detachment limit, or it detaches during the first milliseconds after the pneumatic action or it does not detach at all.

Figure 34 – Needle acceleration during the droplet detachment for an experimental point; the black line indicates the instant of pneumatic activation.

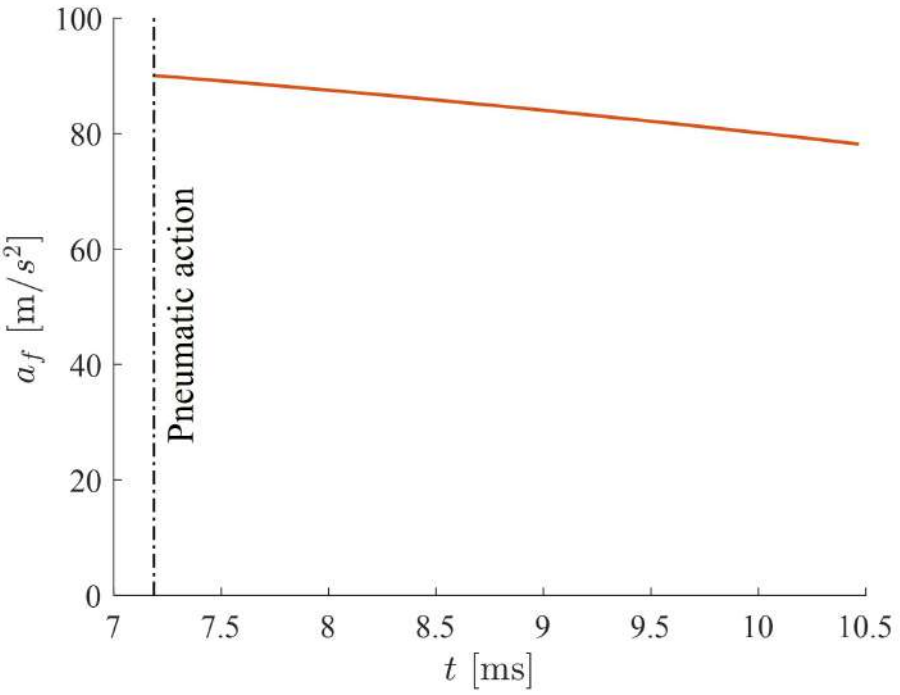

The same procedure was executed for 20 experimental data, reported in Table 2. It indicates the droplet diameter and the needle acceleration range during the detachment. Pneumatic pressures of 1 and 4 bar were utilized obtaining different acceleration values. The chosen needle diameter was the inner ($d_0 = 82.6$ μm) as the visual analysis indicated for the liquid contact of minor droplets. The supplier did not provide uncertainties for the needle diameter measurements.

Utilizing those experimental points, a comparison between the data and the model could be made, as illustrated in Figure 35. Each dot represents an experimental point and their colors indicate if the droplet detached or not. The red and green regions represent the droplet detachment predicted by the model, in which red is for undetached droplets and green is for detached droplets. As the acceleration during the process is not constant, the average value between the maximum and minimum accelerations was utilized and the error bars indicated their ranges. Analyzing the results, only two average value points do not agree with the model, but their ranges do. Therefore, it was reasonable to consider that the droplet generator worked as expected, providing minor droplets (from 547 μm), but more controlled tests were necessary to validate the model.

Table 2 – First experimental data for the droplet detachment model validation, using water and a 34G hypodermic needle.

Droplet detachment	d [μm]	$a_{f,min}$ [g]	$a_{f,max}$ [g]
No	340	2.01	9.46
No	607	2.73	10.69
No	755	3.42	11.12
No	769	1.18	8.75
No	779	1.57	8.63
Yes	823	2.20	9.33
Yes	824	1.76	8.34
Yes	872	1.89	8.91
Yes	915	1.70	9.18
Yes	1051	1.27	8.17
Yes	1590	3.76	12.30
No	290	7.84	22.42
No	424	8.73	24.71
No	487	9.26	23.95
Yes	547	10.25	26.63
Yes	590	10.39	24.45
Yes	778	8.38	24.58
Yes	823	8.43	23.27
Yes	895	6.80	25.96
Yes	900	7.38	24.27

Figure 35 – Graph comparison between the model and the experimental data for droplet detachment; the colored regions indicate the model prediction – red for undetached droplets and green for detached droplets.

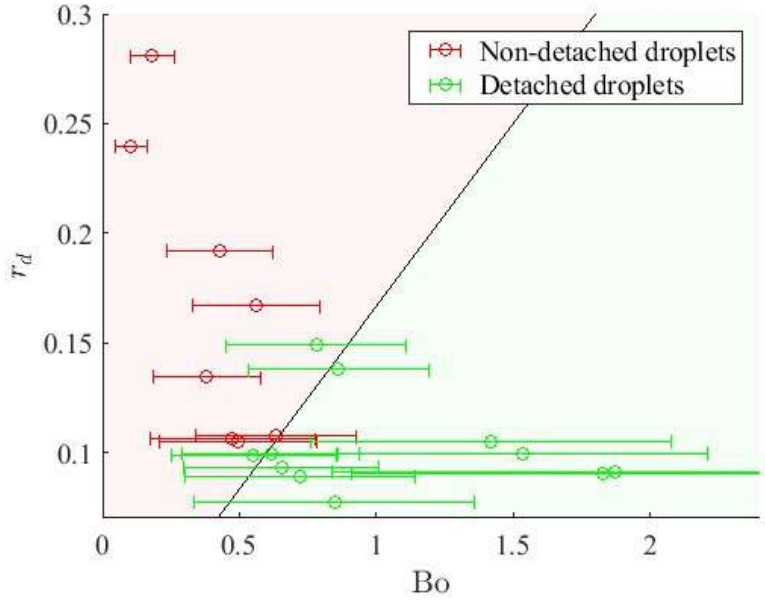

4.2 Droplet detachment model validation

Aiming to validate the proposed model, an extensive battery of tests was executed, providing 136 new experimental points for water under more controlled conditions than those from the previous section. The experiments included four different industrial needles – i.e., with a flat tip. Those needles provide an axisymmetric distribution of the surface tension forces, agreeing with the proposed model. Figure 36 presents images from two experiments for a 30G needle: the minor droplet, on the left-hand side, has not detached whereas the major droplet, on the right-hand side, has detached. As the industrial needles are longer than the hypodermic ones, the needle base could not be utilized for position tracking as in the first experiments. Therefore, a small piece of silicon was attached to the outer diameter of the needles so it could be utilized as a reference for the vertical position.

Figure 36 – Frames for two experimental data, using a 30G industrial needle and water.

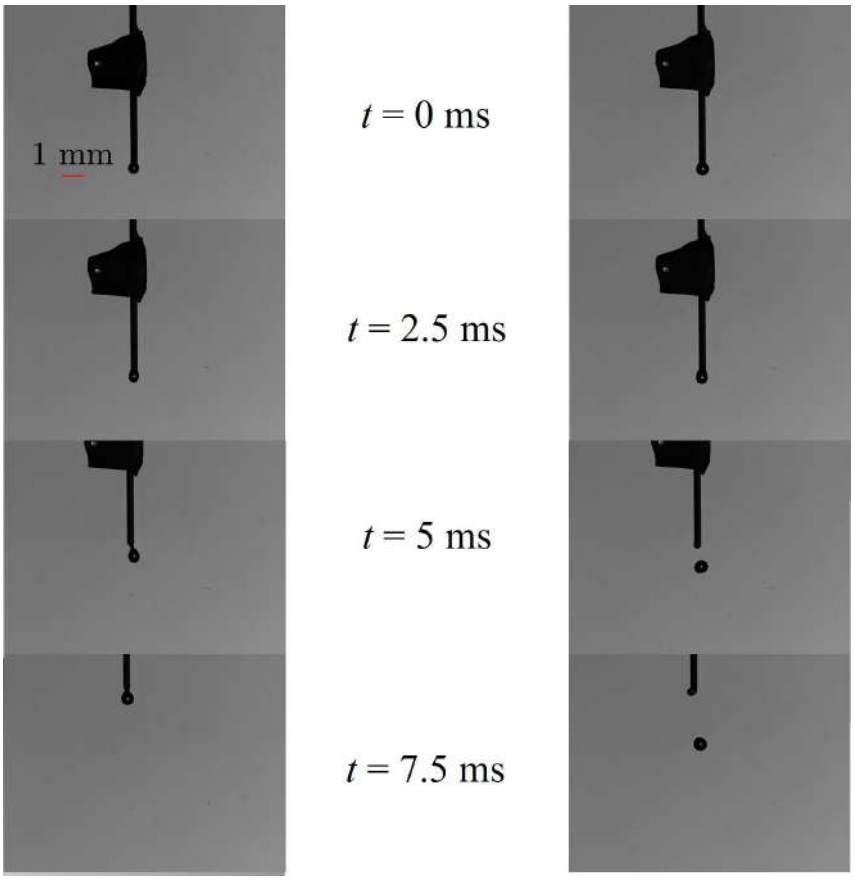

Figure 37 presents images from two experiments for a 24G needle, utilizing the same air pressure (5.58 bar). In this case, the pneumatic action caused a jet generation as the inner diameter and the acceleration of the needle were sufficiently large. Therefore, the experimental analysis was limited to needle sizes smaller than 24G (specifically, 34, 30, and 26G models), since no results could be obtained for that diameter. It must be noticed

that needles with higher gauge values are thinner, with the 34G model being the thinnest in the industry.

Figure 37 – Frames for two experimental data, using a 24G industrial needle and water; droplets could not be properly generated using this needle size.

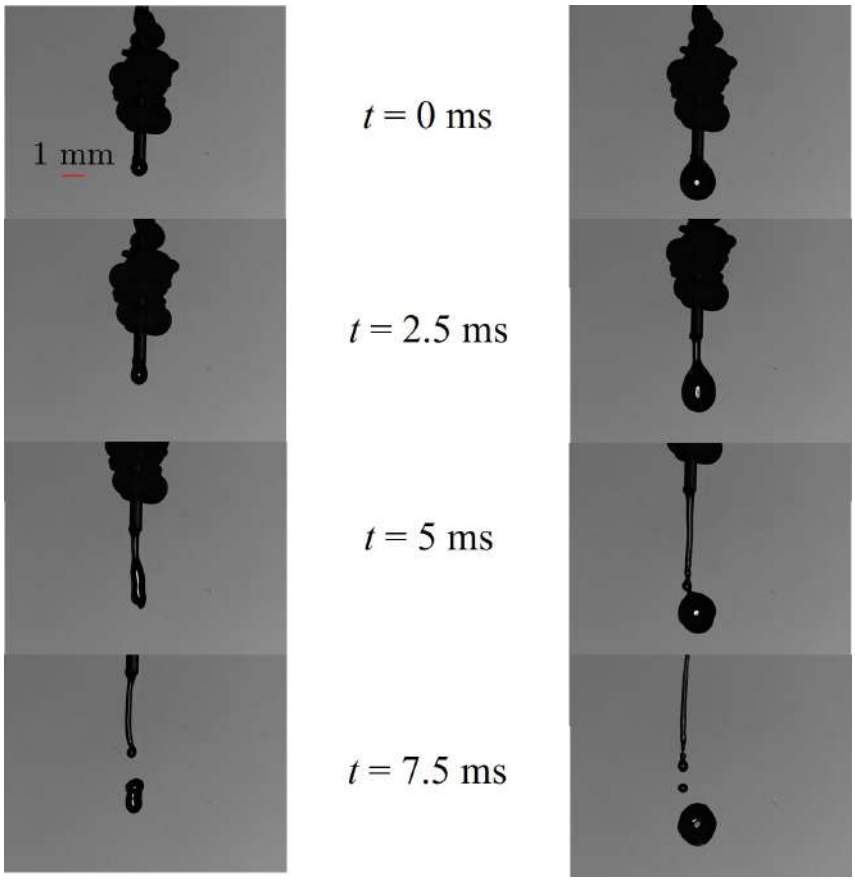

Figure 38 illustrates the needle's tracking position and the fourth-degree polynomial adjustment for one of the 26G experiments. As before, the polynomial was adjusted considering only the interval of the needle movement, excluding the instants before the pneumatic activation. However, the vertical distance until the needle left the image was smaller when compared to the first experiments, as the camera was moved closer to the droplet providing a better pixel resolution. Figure 39 illustrates the needle's tracking velocity, which was calculated as the first derivative of the adjusted polynomial. The velocity values were higher than the first results as the pneumatic pressure was also higher (5.58 bar now against 4 bar before).

Figure 40 illustrates the needle acceleration profile for the same experiment. The curve was obtained considering the second derivative of the adjusted polynomial. For the experiments where the droplet was detached, the acceleration was calculated until the detachment frame whereas for undetached droplets the acceleration was computed for all the vertical trajectory. It can be noticed that the acceleration considerably varied during droplet detachment, decreasing by half throughout the movement.

Figure 38 – Needle position during the droplet detachment for an experimental point; the red curve indicates the fourth-degree polynomial adjustment whereas the black line indicates the instant of pneumatic activation.

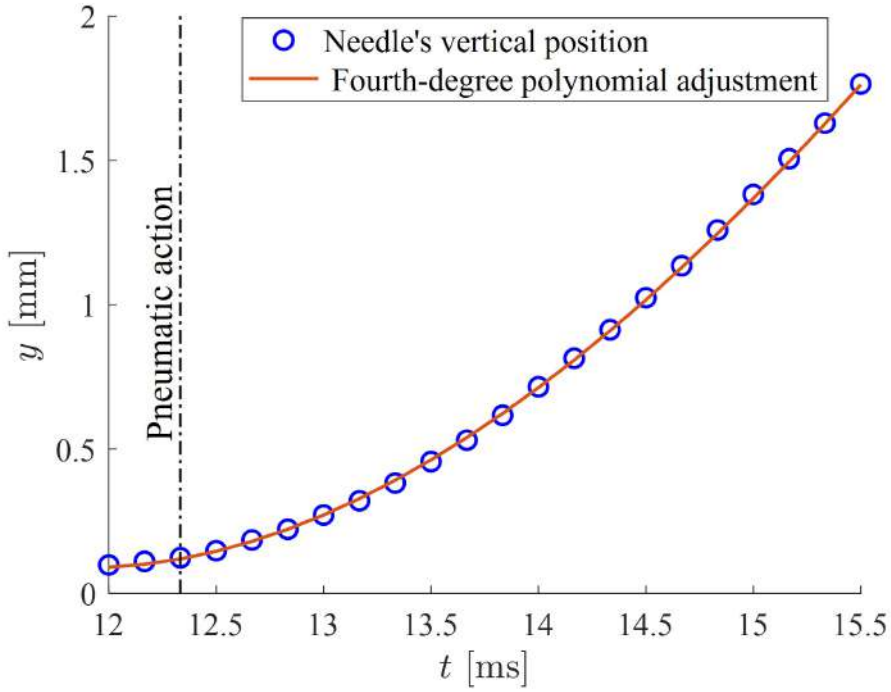

Figure 39 – Needle velocity during the droplet detachment for an experimental point; the black line indicates the instant of pneumatic activation.

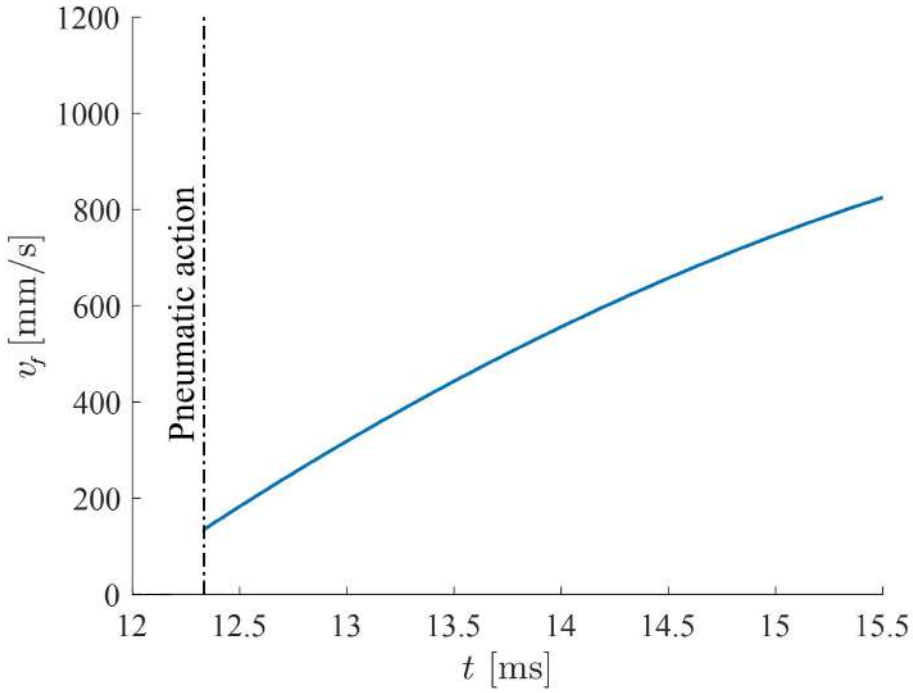

Figure 40 – Needle acceleration during the droplet detachment for an experimental point; the black line indicates the instant of pneumatic activation.

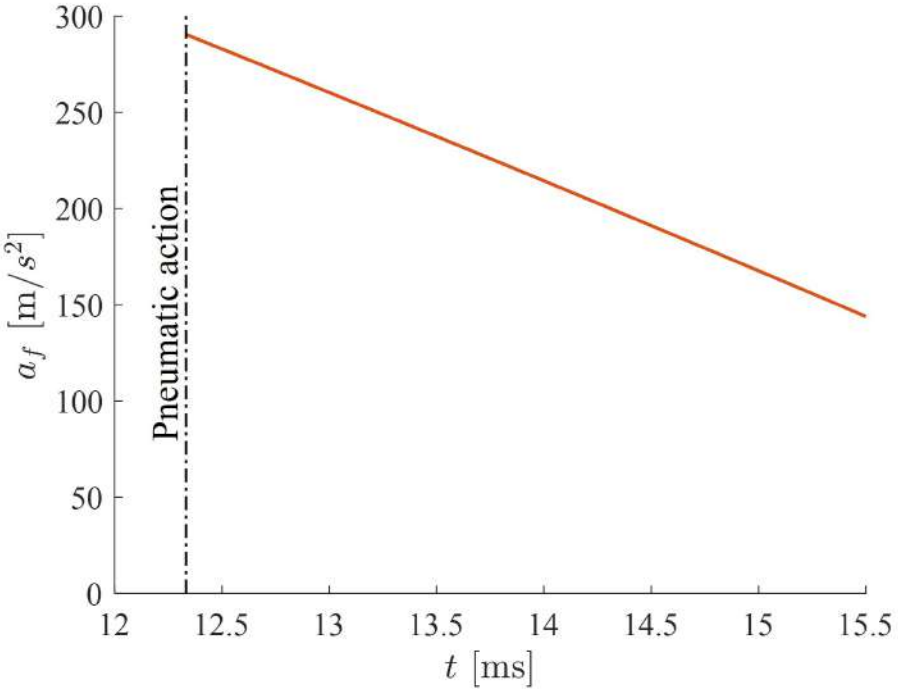

The same procedure was done for the other experimental points. Pneumatic pressures of 2.76 and 5.58 bar were utilized. The chosen needle diameters were the inner values reported by the needle's supplier. All the experimental data are reported in Appendix B. Utilizing those experimental points, a comparison between the data and the model could be made, as illustrated in Figure 41. Each dot represents an experimental point and their colors indicate if the droplet detached or not. The red and green regions represent the droplet detachment predicted by the model, in which red is for undetached droplets and green is for detached droplets once again. As the acceleration during the process is not constant, the average value between the maximum and minimum accelerations was utilized and the error bars indicated their ranges. 15 experimental points of detached droplets had Bond numbers greater than 10 and did not appear on the graph – as the focus of the analysis was comparing the experimental data to the model, the plot was considered until Bo = 10 for a better resolution of the droplets next to the theoretical limit. Once again, only four points had their total range out of the expected area, all undetached droplets from a 34G needle. As mentioned, a large uncertainty is associated with its needle size measurements, requiring more careful analysis. Figure 42 compares the use of different needle sizes in r_d, specifically the inner diameter of 60 μm, on the left-hand side, and an intermediate diameter of 120 μm, on the right-hand side. When changing the diameter from 60 to 120 μm all four points adjust to the model, enabling a complete agreement between the experimental data and the physical model. This research could not identify in which diameter the fluid attaches with the available resources; therefore, the

actual adjustment of the experimental data remains unclear, and further investigations regarding the solid-liquid contact are needed. For now, the best hypothesis is that the fluid attaches to the inner diameter, which provides a great agreement with the physical model.

Figure 41 – Graph comparison between the model and the experimental data for droplet detachment; the colored regions indicate the model prediction – red for undetached and green for detached droplets.

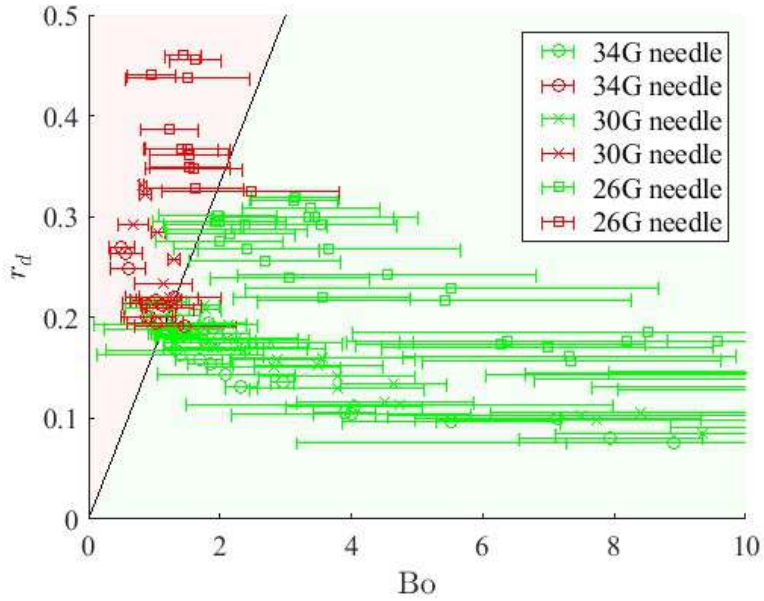

Figure 42 – Graph comparison between the model and the experimental data, for two different attachment diameters.

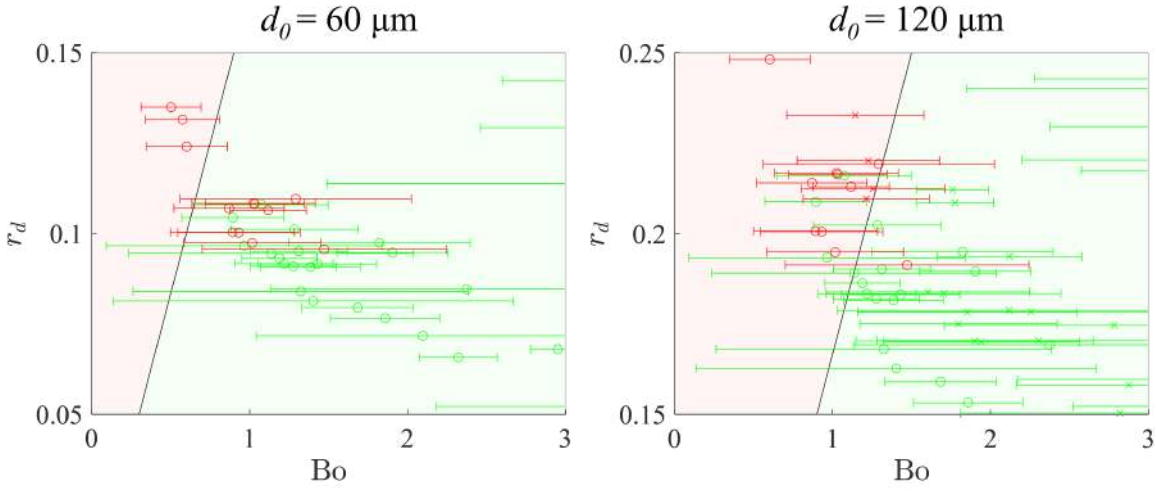

Figure 43 illustrates the minimum detached droplet diameter obtained for each experimental condition. As expected, the droplet minimum diameter decreased as thinner

needles were utilized; moreover, higher pneumatic pressure provided larger needle accelerations resulting in smaller droplets.

Figure 43 – Minimal detached droplet diameter obtained for each experimental condition.

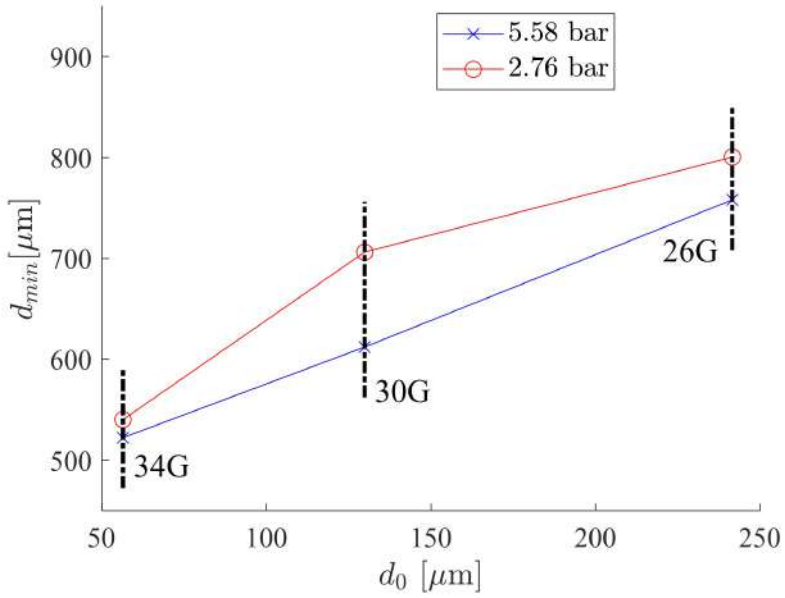

5 CONCLUSIONS

This final-year project proposed the experimental study of a droplet detachment model. An extensive study of the literature on droplet generators was executed to find the most appropriate solution to be used in the research group's experiments. An experimental apparatus was developed and mounted, from which 136 experimental points were obtained for different test conditions. Finally, the experimental data were compared to the theoretical model, with only four deviating experimental points (3%). When mounted with the thinner needle (34G), the droplet generator produced droplets with diameters ranging from 522 to 2100 μm. Moreover, the minimum droplet size graph validated the concept of the droplet generator built, which contributes to the research group to which this work is related, as such equipment is necessary for studies of droplet impact with varying droplet sizes.

Further investigation must be considered to improve the precision of the model. The main obstacles remain at the needle acceleration values, as they vary remarkably. A system where a constant acceleration is applied would improve the quality of the results. Further measurements of the needle size are also important, as the uncertainties related to it are high. Finally, an analysis of the characteristic time of detachment could potentialize the results, as the droplet detachment time varies depending on the experimental conditions.

Three conference papers were published in the context of the undergraduate research related to this work and a related research internship performed at the University of Lorraine in Nancy, France:

1. J. M. M. Silva Filho, J. N. Santos, A. V. S. Oliveira Development of a monodisperse droplet generator through a physical model for droplet detachment. 31st International Symposium on Scientific and Technological Initiation (SIICUSP), São Carlos, Brazil, 2023 (oral presentation conducted by João Marcelo M. Silva Filho);

2. J. M. M. Silva Filho, G. Castanet, M. Gradeck, A. V. S. Oliveira Characteristics of multiple droplet stream generation using high-speed shadowgraphy. 7th Multiphase Flow Journeys (JEM 2023), Rio de Janeiro, Brazil, 2023 (oral presentation conducted by João Marcelo M. Silva Filho);

3. J. M. M. Silva Filho, G. Castanet, M. Gradeck, A. V. S. Oliveira Characteristics of droplet stream generation for different diameters of the nozzle hole. 7th Multiphase Flow Journeys (JEM 2023), Rio de Janeiro, Brazil, 2023 (oral presentation conducted by Arthur V. S. Oliveira).

BIBLIOGRAPHY

ANFINRUD, P. et al. Visualizing speech-generated oral fluid droplets with laser light scattering. New England Journal of Medicine, Mass Medical Soc, v. 382, n. 21, p. 2061–2063, 2020.

ASHGRIZ, N. Handbook of atomization and sprays: theory and applications. [S.l.]: Springer Science & Business Media, 2011.

BASI, S. et al. Evaluation of a pneumatic drop-on-demand generator for application of agrochemical solutions. Crop protection, Elsevier, v. 40, p. 121–125, 2012.

BAUMGARTEN, C. Mixture formation in internal combustion engines. [S.l.]: Springer Science & Business Media, 2006.

BONHOEFFER, B.; KWADE, A.; JUHNKE, M. Impact of formulation properties and process parameters on the dispensing and depositioning of drug nanosuspensions using micro-valve technology. Journal of pharmaceutical sciences, Elsevier, v. 106, n. 4, p. 1102–1110, 2017.

CARROLL, B. J. et al. Differences in surface tensions of non-ionic surfactant solutions as measured by the drop-volume and wilhelmy-plate techniques. Journal of the Chemical Society, Faraday Transactions 1: Physical Chemistry in Condensed Phases, Royal Society of Chemistry, v. 81, n. 12, p. 2975–2980, 1985.

CASTREJÓN-PITA, J. et al. A simple large-scale droplet generator for studies of inkjet printing. Review of Scientific Instruments, AIP Publishing, v. 79, n. 7, 2008.

CHEN, P.-H. et al. Droplet formation of a thermal sideshooter inkjet printhead. International Journal of heat and fluid flow, Elsevier, v. 19, n. 4, p. 382–390, 1998.

CHENG, S.; CHANDRA, S. A pneumatic droplet-on-demand generator. Experiments in fluids, Springer, v. 34, p. 755–762, 2003.

CHENG, S. X.; LI, T.; CHANDRA, S. Producing molten metal droplets with a pneumatic droplet-on-demand generator. journal of materials processing technology, Elsevier, v. 159, n. 3, p. 295–302, 2005.

COLLINS, R. T.; HARRIS, M. T.; BASARAN, O. A. Breakup of electrified jets. Journal of Fluid Mechanics, Cambridge University Press, v. 588, p. 75–129, 2007.

CROWLEY, J. M. Electrohydrodynamic droplet generators. Journal of Electrostatics, Elsevier, v. 14, n. 2, p. 121–134, 1983.

DABORA, E. K. Production of monodisperse sprays. Review of Scientific Instruments, AIP Publishing, v. 38, n. 4, p. 502–506, 1967.

DONNELLY, R. J.; GLABERSON, W. Experiments on the capillary instability of a liquid jet. Proceedings of the Royal Society of London. Series A. Mathematical and Physical Sciences, The Royal Society London, v. 290, n. 1423, p. 547–556, 1966.

DOU, R.; WEN, Z.; ZHOU, G. Heat transfer characteristics of water spray impinging on high temperature stainless steel plate with finite thickness. International Journal of Heat and Mass Transfer, Elsevier, v. 90, p. 376–387, 2015.

DUMOUCHEL, C. On the experimental investigation on primary atomization of liquid streams. Experiments in fluids, Springer, v. 45, p. 371–422, 2008.

EARNSHAW, J. et al. The drop volume method for interfacial tension determination: an error analysis. Journal of colloid and interface science, Elsevier, v. 177, n. 1, p. 150–155, 1996.

FAN, K.-C. et al. Development of a drop-on-demand droplet generator for one-drop-fill technology. Sensors and Actuators A: Physical, Elsevier, v. 147, n. 2, p. 649–655, 2008.

GOGHARI, A. A.; CHANDRA, S. Producing droplets smaller than the nozzle diameter by using a pneumatic drop-on-demand droplet generator. Experiments in Fluids, Springer, v. 44, p. 105–114, 2008.

HARKINS, W. D.; BROWN, F. The determination of surface tension (free surface energy), and the weight of falling drops: The surface tension of water and benzene by the capillary height method. Journal of the American Chemical Society, ACS Publications, v. 41, n. 4, p. 499–524, 1919.

HIROYASU, H.; ARAI, M. Structures of fuel sprays in diesel engines. SAE transactions, JSTOR, p. 1050–1061, 1990.

HRDINA, D. W.; CROWLEY, J. M. Drop-on-demand operation of continuous jets using ehd techniques. IEEE transactions on industry applications, IEEE, v. 25, n. 4, p. 705–710, 1989.

JIANG, Y.; UMEMURA, A.; LAW, C. K. An experimental investigation on the collision behaviour of hydrocarbon droplets. Journal of Fluid Mechanics, Cambridge University Press, v. 234, p. 171–190, 1992.

KIM, Y.-J. et al. Drop-on-demand hybrid printing using a piezoelectric mems printhead at various waveforms, high voltages and jetting frequencies. Journal of Micromechanics and Microengineering, IOP Publishing, v. 23, n. 6, p. 065011, 2013.

KOSCH, S.; ASHGRIZ, N. Note: A simple vibrating orifice monodisperse droplet generator using a hard drive actuator arm. Review of Scientific Instruments, AIP Publishing, v. 86, n. 4, 2015.

LE, H. P. Progress and trends in ink-jet printing technology. Journal of imaging science and technology, Society for Imaging Science and Technology, v. 42, n. 1, p. 49–62, 1998.

LEE, B.-B.; RAVINDRA, P.; CHAN, E.-S. A critical review: surface and interfacial tension measurement by the drop weight method. Chemical Engineering Communications, Taylor & Francis, v. 195, n. 8, p. 889–924, 2008.

LEE, B.-B.; RAVINDRA, P.; CHAN, E.-S. New drop weight analysis for surface tension determination of liquids. Colloids and Surfaces A: Physicochemical and Engineering Aspects, Elsevier, v. 332, n. 2-3, p. 112–120, 2009.

LEFEBVRE, A. H.; MCDONELL, V. G. Atomization and sprays. [S.l.]: CRC press, 2017.

LEMKE, R. E.; HIEFTJE, G. M. A new, directly computer-controlled ph-stat. Analytica Chimica Acta, Elsevier, v. 141, p. 173–186, 1982.

LIN, S. P.; REITZ, R. D. Drop and spray formation from a liquid jet. Annual review of fluid mechanics, Annual Reviews 4139 El Camino Way, PO Box 10139, Palo Alto, CA 94303-0139, USA, v. 30, n. 1, p. 85–105, 1998.

MINOV, S. V. et al. Droplet generation and characterization using a piezoelectric droplet generator and high speed imaging techniques. Crop Protection, Elsevier, v. 69, p. 18–27, 2015.

MISHRA, S. et al. High-speed and drop-on-demand printing with a pulsed electrohydrodynamic jet. Journal of Micromechanics and Microengineering, IOP Publishing, v. 20, n. 9, p. 095026, 2010.

MOREIRA, A.; MOITA, A.; PANAO, M. Advances and challenges in explaining fuel spray impingement: How much of single droplet impact research is useful? Progress in energy and combustion science, Elsevier, v. 36, n. 5, p. 554–580, 2010.

OHNESORGE, W. v. The formation of drops by nozzles and the breakup of liquid jets. 2019.

PLATEAU, M. Xxxvii. on the recent theories of the constitution of jets of liquid issuing from circular orifices. The London, Edinburgh, and Dublin Philosophical Magazine and Journal of Science, Taylor & Francis, v. 12, n. 79, p. 286–297, 1856.

RAYLEIGH, L. On the capillary phenomena of jets. Proceedings of the royal society of London, JSTOR, p. 71–97, 1879.

REITZ, R. D. Atomization and other breakup regimes of a liquid jet. [S.l.]: Princeton University, 1978.

SAVART, F. Wemoire sur la constitution des veines liquids lancees par des orifices circulaires en mince paroi. Ann. de chim., v. 53, p. 337–386, 1833.

SINGH, M. et al. Inkjet printing—process and its applications. Advanced materials, Wiley Online Library, v. 22, n. 6, p. 673–685, 2010.

TATE, T. Xxx. on the magnitude of a drop of liquid formed under different circumstances. The London, Edinburgh, and Dublin Philosophical Magazine and Journal of Science, Taylor & Francis, v. 27, n. 181, p. 176–180, 1864.

TAYLOR, G. I. The coalescence of closely spaced drops when they are at different electric potentials. Proceedings of the Royal Society of London. Series A. Mathematical and Physical Sciences, The Royal Society London, v. 306, n. 1487, p. 423–434, 1968.

TRETTEL, B. Reevaluating the jet breakup regime diagram. Atomization and Sprays, Begel House Inc., v. 30, n. 7, 2020.

WANG, C.; LIU, X.; LAW, C. Combustion and microexplosion of freely falling multicomponent droplets. Combustion and flame, Elsevier, v. 56, n. 2, p. 175–197, 1984.

WANG, L. et al. Experimental investigation on the performances of a valve-based and on-demand droplet generator producing droplets in a wide size range. AIP Advances, AIP Publishing, v. 12, n. 9, 2022.

WEBER, C. Zum zerfall eines flüssigkeitsstrahles. ZAMM-Journal of Applied Mathematics and Mechanics/Zeitschrift für Angewandte Mathematik und Mechanik, Wiley Online Library, v. 11, n. 2, p. 136–154, 1931.

WILKINSON, M. Extended use of, and comments on, the drop-weight (drop-volume) technique for the determination of surface and interfacial tensions. Journal of Colloid and Interface Science, Elsevier, v. 40, n. 1, p. 14–26, 1972.

WU, H.; ZHANG, F.; ZHANG, Z. Fundamental spray characteristics of air-assisted injection system using aviation kerosene. Fuel, Elsevier, v. 286, p. 119420, 2021.

WU, X. et al. Dual-stream of monodisperse droplet generator. Chemical Engineering Science, Elsevier, v. 223, p. 115645, 2020.

YANG, J. C. et al. A simple piezoelectric droplet generator. Experiments in fluids, Springer, v. 23, n. 5, p. 445–447, 1997.

YIWEI, W. et al. Generation of micro-droplet on demand with reduced sizes by a hybrid pneumatic electrohydrodynamic method. Journal of Micromechanics and Microengineering, IOP Publishing, v. 30, n. 3, p. 035002, 2020.

YOUNG, T. Iii. an essay on the cohesion of fluids. Philosophical transactions of the royal society of London, The Royal Society London, n. 95, p. 65–87, 1805.

ZHANG, T. et al. Advanced study of spray cooling: from theories to applications. Energies, MDPI, v. 15, n. 23, p. 9219, 2022.

ZOLTAN, S. I. Pulsed droplet ejecting system. [S.l.]: Google Patents, 1972. US Patent 3,683,212.

APPENDIX A – MATLAB CODE

```
%% Returns the droplet and needle position evolutions
for a given set of frames:
% Clears the data set:
clear
close all

%% Initial definitions:
% Important parameters:
calibration_number = 1;
scale = pixel_calibration(calibration_number);
polyfit_adjustment = 5*scale;

jumping_criteria = 40;
frame_rate = 6400;

binarize_level = 0.015;
radius_range = [20, 50];
cut_1 = 200;
cut_2 = 100;

% Image directory:
files = dir("\*.tif");
nf = length(files);

figure(1)
hold on

% Data acquisition matrix (needle):
needle_data = zeros(2,nf);

% Data acquisition matrix (droplet):
droplet_data = zeros(3,nf);

%% Image treatment:
for i = 1:nf
    % Reads filename:
```

```
file_name = strcat("\",files(i).name);

% Reads image:
Im = imread(file_name);

% Image cut:
[sy, sx] = size(Im);
Im = Im(1:sy,cut_1:sx-cut_2);
[sy, sx] = size(Im);

% Finds circles:
[centers,radii] = imfindcircles(Im,radius_range,
'ObjectPolarity','dark');

% Binarizes the image:
Im_bin = imbinarize(Im,binarize_level);

% Image visualization:
imshow(Im,[])
viscircles(centers,radii);
text(15,15,strcat("Time: ",string(round(1000*i/frame_rate,2)),
"ms"),'Color','Yellow','FontSize',10)

% Droplet data storage:
if centers ~= 0
    droplet_data(1,i) = centers(1,1);
    droplet_data(2,i) = centers(1,2);
    droplet_data(3,i) = 2*radii;
end

%% Coordinates detection:

% First frame:
if i == 1
    % Reference coordinates:
    ref_y0 = sy/2;
    for j = 1:sx
        if Im_bin(ref_y0,j) == 0
            ref_x0 = j;
```

```
            break
        end
    end

    % Transition coordinates:
    flag = 0;
    for j = ref_y0:-1:1
        for k = 1:sx
            if Im_bin(j,k) == 0 && ref_x0-k >= jumping_criteria
                coord_x0 = k;
                coord_y0 = j;

                needle_data(1,i) = k;
                needle_data(2,i) = j;

                reference_jump = 0;
                flag = 1;
                break
            end
        end
        if flag == 1
            break
        end
    end

%Next frames:
else
    % New reference coordinates:
    ref_y1 = ref_y0 - reference_jump;
    for j = 1:sx
        if Im_bin(ref_y1,j) == 0
            ref_x1 = j;
            break
        end
    end

    % New transition coordinates:
    flag = 0;
    for j = ref_y1:-1:1
```

```
            for k = 1:sx
                if Im_bin(j,k) == 0 && ref_x1-k >= jumping_criteria
                    coord_x1 = k;
                    coord_y1 = j;

                    needle_data(1,i) = k;
                    needle_data(2,i) = j;

                    reference_jump = reference_jump + coord_y0-j;
                    coord_y0 = j;
                    flag = 1;
                    break
                end
            end
            if flag == 1
                break
            end
        end
    end

    % Display coordinate points:
    if i ~= 1
        text(ref_x1,ref_y1,'x','Color','Red','FontSize',10)
        text(coord_x1,coord_y1,'x','Color','Yellow','FontSize',10)
        drawnow
    end
end
hold off

%% Units adjustment:
% Aplies scale:
needle_data = needle_data*scale;
droplet_data = droplet_data*scale;

% Remove frames in which there is no droplet:
i = 1;
j = size(droplet_data,2);

while i <= j
```

```
    if droplet_data(3,i) == 0
        droplet_data(:,i) = [];
        i = i - 1;
        j = j - 1;
    end
    i = i + 1;
end

% Remove the last 4 frames (droplet):
for i = size(droplet_data,2):-1:size(droplet_data,2)-3
    droplet_data(:,i) = [];
end

% Remove frames in which there is no needle:
i = 1;
j = size(needle_data,2);

while i <= j
    if needle_data(2,i) == 0
        needle_data(:,i) = [];
        i = i - 1;
        j = j - 1;
    end
    i = i + 1;
end

% Puts the values in ascending order (needle):
for i = 2:size(needle_data,2)
    needle_data(2,i) = needle_data(2,1)-needle_data(2,i);
end

needle_data(2,1) = 0;

%% Plotage adjustments:
% Time adjustments, in seconds:
n = max(size(needle_data,2),size(droplet_data,2));
time = zeros(1,n);

for i = 1:length(time)
```

```
    time(i) = (i/frame_rate);
end

%% Plots needle vertical position evolution:
% Finds the initial point for polynomial adjustment:
for i = 2:size(needle_data,2)
    if needle_data(2,i) >= polyfit_adjustment
        h = i;
        size_criteria = 2*i-50;
        break
    end
end

% Polynomial fitting (position):
position_coefficients = polyfit(time(h:size(needle_data,2)),
needle_data(2,(h:size(needle_data,2))),4);
position_values = polyval(position_coefficients,
time(1:size(needle_data,2)));

% Polynomial fitting (velocity):
velocity_coefficients = position_coefficients(1:end-1).*
(length(position_coefficients)-1:-1:1);
velocity_values = polyval(velocity_coefficients,
time(1:size(needle_data,2)));
velocity_values(1:h-1) = 0;

% Polynomial fitting (acceleration):
acceleration_coefficients = velocity_coefficients(1:end-1).*
(length(velocity_coefficients)-1:-1:1)/1000;
acceleration_values = polyval(acceleration_coefficients,
time(1:size(needle_data,2)));
acceleration_values(1:h-1) = 0;

position_y_droplet = polyfit(time(128:size(droplet_data,2)),
1000*droplet_data(2,(128:size(droplet_data,2))),2);
p_y_values = polyval(position_y_droplet,
time(128:size(droplet_data,2)));
figure(10)
plot(time(1:size(droplet_data,2)),droplet_data(2,:))
```

```
% Plots results for position:
figure(2)
plot(time(1:size(needle_data,2))*1000,needle_data(2,:),
'.b',time(1:size(needle_data,2))*1000,position_values)
grid on
axis auto
title('Coordenada vertical da agulha $versus$ Tempo',
'interpreter','latex')
xlabel('Tempo $(ms)$','interpreter','latex')
ylabel('Coordenada vertical $(mm)$','interpreter','latex')
legend("Coordenada vertical real","Ajuste polyfit")

% Plots results for velocity:
figure(3)
plot(time(1:size(needle_data,2)),velocity_values)
grid on
axis auto
title('Needle Velocity $versus$ Time','interpreter','latex')
xlabel('Time $(s)$','interpreter','latex')
ylabel('Velocity $(\frac{mm}{s})$','interpreter','latex')

% Plots results for acceleration:
figure(4)
plot(time(1:size(needle_data,2))*1000,acceleration_values)
grid on
axis auto
title('Aceleracao da Agulha $versus$ Tempo','interpreter','latex')
xlabel('Tempo $(ms)$','interpreter','latex')
ylabel('Aceleracao $(\frac{m}{s^2})$','interpreter','latex')

disp(max(acceleration_values)/9.81)

disp(min(acceleration_values(acceleration_values>0))/9.811590)


%% Plots droplet size evolution:
% Finds droplet mean diameter:
mean_diameter = mean(droplet_data(3,
```

```
(size_criteria:size(droplet_data,2))));
flag = sprintf('Droplet mean diameter: %d( m )',
1000*round(mean_diameter,3));
disp(flag)

% Plotage adjustments:
figure(5)
plot(time(1:size(droplet_data,2)),droplet_data(3,:))
line([time(size_criteria),time(size_criteria)],
[min(droplet_data(3,:)),max(droplet_data(3,:))],
'Color','red','LineWidth',1,'LineStyle','-.')

grid on
axis auto
title('Droplet Diameter $versus$ Time','interpreter','latex')
xlabel('Time $(s)$','interpreter','latex')
ylabel('Droplet Diameter $(mm)$','interpreter','latex')
```

APPENDIX B – EXPERIMENTAL DATA

d_0 [G]	Air pressure [bar]	d [mm]	Droplet detachment	$a_{f,min}$ [m/s^2]	$a_{f,max}$ [m/s^2]
34	5.58	1.413	Yes	230.165	331.770
34	5.58	1.162	Yes	199.503	377.871
34	5.58	1.122	Yes	277.581	530.544
34	5.58	1.014	Yes	203.975	351.026
34	5.58	1.486	Yes	230.659	338.918
34	5.58	1.081	Yes	126.682	353.322
34	5.58	0.786	Yes	113.456	362.718
34	5.58	0.829	Yes	285.384	322.221
34	5.58	0.693	Yes	10.827	396.047
34	5.58	0.597	Yes	38.512	408.325
34	5.58	0.671	Yes	32.712	377.093
34	5.58	0.584	Yes	9.910	384.758
34	5.58	0.520	No	161.331	372.371
34	5.58	0.521	No	183.733	351.370
34	5.58	0.522	Yes	164.542	391.362
34	5.58	0.593	Yes	198.951	326.398
34	5.58	0.530	No	218.286	343.878
34	5.58	0.514	No	144.666	548.821
34	5.58	0.579	Yes	262.630	513.312
34	5.58	0.595	Yes	310.438	455.463
34	2.76	0.858	Yes	196.278	245.065
34	2.76	1.072	Yes	207.700	268.264
34	2.76	0.736	Yes	194.053	287.379
34	2.76	0.616	Yes	193.592	337.752
34	2.76	0.621	Yes	192.522	312.226
34	2.76	0.455	No	112.331	293.804
34	2.76	0.557	Yes	197.163	386.813
34	2.76	0.667	Yes	176.245	584.681
34	2.76	0.429	No	125.530	312.089
34	2.76	0.605	Yes	179.862	274.566
34	2.76	0.563	No	115.937	294.618
34	2.76	0.620	Yes	181.097	284.695
34	2.76	0.418	No	120.791	279.969
34	2.76	0.527	No	127.114	310.547

34	2.76	0.579	No	117.454	306.242
34	2.76	0.562	No	105.737	287.186
34	2.76	0.615	Yes	164.902	285.269
34	2.76	0.590	No	137.308	461.718
34	2.76	0.709	Yes	183.442	286.002
34	2.76	0.540	Yes	133.102	294.957
30	5.58	1.727	Yes	67.796	457.221
30	5.58	1.976	Yes	338.538	453.013
30	5.58	1.422	Yes	309.738	635.144
30	5.58	0.813	Yes	229.769	537.826
30	5.58	0.744	Yes	215.637	499.818
30	5.58	1.651	Yes	284.561	462.539
30	5.58	2.023	Yes	318.759	416.453
30	5.58	1.220	Yes	290.202	515.830
30	5.58	0.912	Yes	218.691	426.711
30	5.58	0.404	No	339.877	415.640
30	5.58	0.967	Yes	289.312	415.508
30	5.58	0.623	Yes	278.462	370.636
30	5.58	0.853	Yes	243.309	440.002
30	5.58	0.457	No	321.307	397.554
30	5.58	0.503	No	339.023	394.758
30	5.58	1.141	Yes	73.862	437.974
30	5.58	0.670	Yes	260.411	409.131
30	5.58	0.392	No	362.586	393.133
30	5.58	0.821	Yes	224.547	379.471
30	5.58	0.612	Yes	289.418	377.853
30	2.76	1.322	Yes	211.113	415.656
30	2.76	1.536	Yes	210.364	348.584
30	2.76	1.268	Yes	197.188	465.133
30	2.76	1.119	Yes	174.771	332.631
30	2.76	1.004	Yes	168.335	359.497
30	2.76	0.708	Yes	130.053	346.809
30	2.76	0.558	No	156.853	360.451
30	2.76	0.728	Yes	149.907	452.276
30	2.76	0.726	Yes	132.835	433.710
30	2.76	0.706	Yes	130.775	319.527
30	2.76	0.728	Yes	149.685	340.848

30	2.76	0.742	Yes	145.803	311.607
30	2.76	0.445	No	153.325	322.729
30	2.76	0.764	Yes	155.780	310.942
30	2.76	0.590	No	153.095	342.343
30	2.76	0.611	No	146.643	324.458
30	2.76	0.864	Yes	167.511	365.330
30	2.76	0.762	Yes	151.506	408.406
30	2.76	0.620	No	145.069	297.126
30	2.76	0.762	Yes	134.351	323.137
26	5.58	1.688	Yes	145.516	626.621
26	5.58	1.907	Yes	207.219	544.098
26	5.58	2.055	Yes	244.634	573.465
26	5.58	1.653	Yes	201.757	517.863
26	5.58	1.368	Yes	174.761	445.409
26	5.58	1.365	Yes	183.766	546.429
26	5.58	1.304	Yes	163.211	549.035
26	5.58	1.111	Yes	142.727	479.193
26	5.58	1.052	Yes	146.958	561.932
26	5.58	0.903	Yes	139.892	495.768
26	5.58	0.807	Yes	201.368	553.675
26	5.58	0.530	No	309.139	514.516
26	5.58	0.782	Yes	269.183	520.319
26	5.58	0.995	Yes	158.368	492.638
26	5.58	0.763	Yes	297.454	466.768
26	5.58	0.758	Yes	305.536	475.241
26	5.58	0.524	No	297.627	444.268
26	5.58	0.552	No	128.158	578.251
26	5.58	0.806	Yes	222.368	512.800
26	5.58	0.829	Yes	241.526	489.675
26	2.76	2.311	Yes	221.043	364.702
26	2.76	1.890	Yes	154.987	453.222
26	2.76	1.834	Yes	156.773	326.896
26	2.76	1.741	Yes	153.847	309.308
26	2.76	1.535	Yes	147.342	288.186
26	2.76	0.876	Yes	88.015	271.263
26	2.76	1.367	Yes	144.127	334.377
26	2.76	1.387	Yes	144.795	311.689

26	2.76	0.902	Yes	106.319	304.673
26	2.76	0.696	No	120.628	343.672
26	2.76	1.096	Yes	123.869	288.514
26	2.76	0.946	Yes	115.753	303.068
26	2.76	1.667	Yes	164.917	343.270
26	2.76	0.548	No	132.494	311.077
26	2.76	0.852	Yes	109.830	306.348
26	2.76	1.418	Yes	152.038	335.973
26	2.76	1.006	Yes	123.499	298.461
26	2.76	1.500	Yes	145.170	309.623
26	2.76	0.826	Yes	111.386	379.062
26	2.76	0.817	Yes	96.530	303.030
26	2.76	0.659	No	133.322	352.692
26	2.76	0.736	No	108.997	309.111
26	2.76	0.800	Yes	112.094	316.712
26	2.76	0.842	Yes	109.412	334.035
26	2.76	0.742	No	139.429	497.205
26	2.76	0.670	No	141.142	336.512
26	2.76	0.692	No	132.625	317.078
26	2.76	0.625	No	136.895	304.503
26	2.76	0.819	Yes	96.234	318.670
26	2.76	0.659	No	135.370	321.896